Hall A Status Report - 2005

Edited by CC

February 2005

Contents

List of Figures

List of Tables

1 Introduction

The beginning of 2005 was marked by an important milestone for hall A, the starting of the physics program with the BigBite spectrometer. The first experiment to use the BigBite spectrometer, E01-015 - Short Range Correlations experiment (spokespersons: W. Bertozzi, E. Piasetzky, J. Watson, S. Wood), began in January 2005 and was succsefully completed in April.

The Hall A Septum magnet pair was reinstalled in the Early Summer following the SRC experiment. The second part the Hyper-nuclear spectroscopy experiment (E-94-107: spokespersons: S. Frullani, F. Garibaldi, J. LeRose, P. Markowitz, T. Saito) was completed in June. The first part of this experiment was conducted in 2004 on ^{12}C and ^{9}Be targets. The 2005 run used the water-fall target, and the HRS par at 6°. In order to achieve high momentum resolution demanded by this experiment, the spectrometer was vacuum coupled to the target. The resulting reduction in multiple scattering allowed the demonstration of the hall A HRS design momentum resolution of less than 1×10^{-4} for the first time.

Hall A parity experiments E99-115 and E00-114 (D. Armstrong, G. Cates, K. Kumar, D. Lhuillier and R. Michaels, Spokespersons) were carried out over the Fall. These experiments used the hall A cryo target the the HRS par at 6° with the septa. While the maximum current possible during the two experiments were limited by continuing septum heating problems, the two experiments were successfully concluded by the end of November.

The installation of the BigBite spectrometer complete with the new detector package, the polarized ^{3}He target and the BigHand neutron detector started in December in preparation for the hall A GEN experiment which is scheduled to start in February 2006.

2 Standard Hall A Facilities

2.1 Septum Magnets

Contributed by John J. LeRose and Paul Brindza

2.1.1 Overview

The two septum magnets (left and right) were manufactured by BWXT Technologies of Lynchburg Virginia under contract with INFN Rome. They were designed to allow access to scattering angles from 6 to 12.5 degrees up to the maximum momentum of each spectrometer with no degradation in the optical properties of either spectrometer (except for some reduction in solid angle acceptance). With the septa in place the target is moved 80 cm upstream from its normal position at the Hall A pivot, precluding the use of one HRS with a septum and the other without.

2.1.2 Developments and Activities in 2005

2005 was a busy year for the septum magnets. After re-installation in the Hall following the SRC experiment in the spring, they were used for production running on E94-107 (Hypernuclear Spectroscopy), E00-114 (HAPPEX-He), and E99-115 (HAPPEX-H).

Throughout, the new EPICS based control system, replacing the radiation damage prone PC controls that came with the magnets, worked very well. However, cryogenics flow in the right septum remains problematic. Surgical investigation into the cryo-flow problem turned up a blockage at the predicted location, but after removal of that blockage coolant flow through the magnet remained low. It is suspected that there is another blockage someplace else. As of this writing there is also another problem, a very leaky control valve. Both the blockage and the leaky valve result in less coolant flow to the magnet and therefore less than optimum cooling. Further investigation and repair will require another surgery which is not likely to happen until more experiments requiring the septum magnets are scheduled.

For E94-107, using thin targets (about 100 mg/cm^2 at beam currents approaching 100 μA), the cryogen flow presented no limitation. During optics commissioning using elastic scattering at 1.85 GeV from Tantalum and Carbon at 6 degrees, momentum resolution of 1e-04 (FWHM) or better was achieved across almost the full momentum acceptance of both left and right arms. The June running was devoted almost exclusively to production running on Oxygen using the waterfall target. For further details and a look at the beautiful spectrum achieved see the status report for E94-107 later in this volume.

For HAPPEX the limited coolant flow in the right septum did contribute to limiting the achievable luminosity. During 2004 HAPPEX was limited to 38 μA while running on the 20 cm Hydrogen target . As noted in last year's annual report, GEANT simulations by Eugene Chudakov indicated that a significant amount of septum heating was the result of very low energy Møller electrons impinging on the bore of the septa. Those studies further indicated that a small sweeping magnet (0.3 T over 0.1 m) would eliminate those electrons with only very little effect on the "good" trajectories (a 3 GeV/c electron is deflected 3 m-rad). Such a sweeping magnet was designed, built, and installed

in the scattering chamber for HAPPEX's 2005 run. In 2005 overheating of the upper coil in the right septum limited the beam current to 58 μA using the 20 cm Hydrogen target, a significant improvement over 2004. Using the 20 cm Helium target the maximum beam current was 38 μA. The difference between running with Hydrogen versus Helium is believed to be extra heating caused by neutrons coming from the Helium which were not included in the simulation.

During 2005 no effort was made to "train" the septum magnets to work at higher currents. Achieved currents were more than adequate for the scheduled program, maximum momentum of 3.1 GeV/c at 6 degrees.

2.2 Status Report on the Cryogenic Target

Contributed by J. P. Chen; Figure by Robert Michaels

The Hall A cryotarget system [1] usually consists of 3 loops: loop 1 is for gaseous helium (either ^{3}He or ^{4}He) at 6-7 K and 15 atm, loop 2 liquid hydrogen at 19K and loop 3 liquid deuterium at 22K. Both the LH_2 and LD_2 loops are operating at pressures above 20 psi. Each of the LH_2 and LD_2 loops usually has two target cells with typical lengths of 15 cm or 4 cm.

In 2005, the cryotarget system was used for three experiments: Short Range Correlation, HAPPEX-II and HAPPEX-He (second period). The Short Range Correlation experiment used the standard target cells (machined 4 and 15 cm 'beer cans'). HAPPEX-II and HAPPEX-He used 20 cm new race-track cells.

During the HAPPEX-II and HAPPEX-He running, loop 1 had a 10 mil thick single race-track cell for high pressure helium running. Loop 2 had a 5 mil thick single race-track cell for liquid hydrogen. The flow is vertical (perpendicular to the beam direction) for the race-track cells.

Due to the added length for the helium running, the maximum 4K cooling power for high beam current running would exceed the End Station Refrigerator limitation. Supplemental cooling from the Central Helium Liquefier (CHL) was needed. The helium target was cooled with 4.2K coolant directly from CHL, with maximum flow of 25 g/s, which was expected to provide enough cooling power for the HAPPEX-He running. Due to another limitation (the beam heating of the Septum magnets), the beam current was restricted to about 38 μA for the HAPPEX-He run period. Even with 38 μA, the cooling power turned out to be another limiting factor, indicating the heat leak of the system is larger than it was before. The operating temperature was initially at 6.7 K and fan speed of 60 Hz. The coolant needed was at 23-24 g/s, pretty close to the maximum. The fan speed was increased to 72 Hz to minimize the density fluctuation. The heat load also increased due to the extra heat power deposited by the fan. Target operating temperature had to be raised to 7.0 K to keep the coolant flow to stay at 23-24 g/s. The target operating pressure was at 200-210 psi. The venting pressure was set at 255 psi to protect the target cell, which was tested to above 300 psi. The target vented a number of times during the whole run period. Initially it was mostly due to the instability of CHL flow because of some over-sensitive settings by the cryogroup to protect the CHL from instability. After discussions between the cryogroup and us, the settings were modified and the coolant flow instability was significantly reduced. Several other venting events were due to IOC reboots, as a result of radiation damage. With the help of the hall technician and the cryotarget group, the target ioc was moved outside the hall and most of the ioc reboots were eliminated. With these improvements, target did vent during the latter part of HAPPEX helium running.

For HAPPEX hydrogen running, ESR provided enough 15K cooling power. Due to Septum heating, the maximum beam current was limited to below 58 μA. Density fluctuations were a major concern for the parity experiments, especially the LH_2 parity JP,do you mean HAPPEX?. To minimize the density fluctuation, the fan speed was increased from the nominal 60 Hz to 91 Hz. A measurement was performed to study the density fluctuations as a function of fan speed and it was found that with the higher fan speed the density fluctuations were significantly reduced.

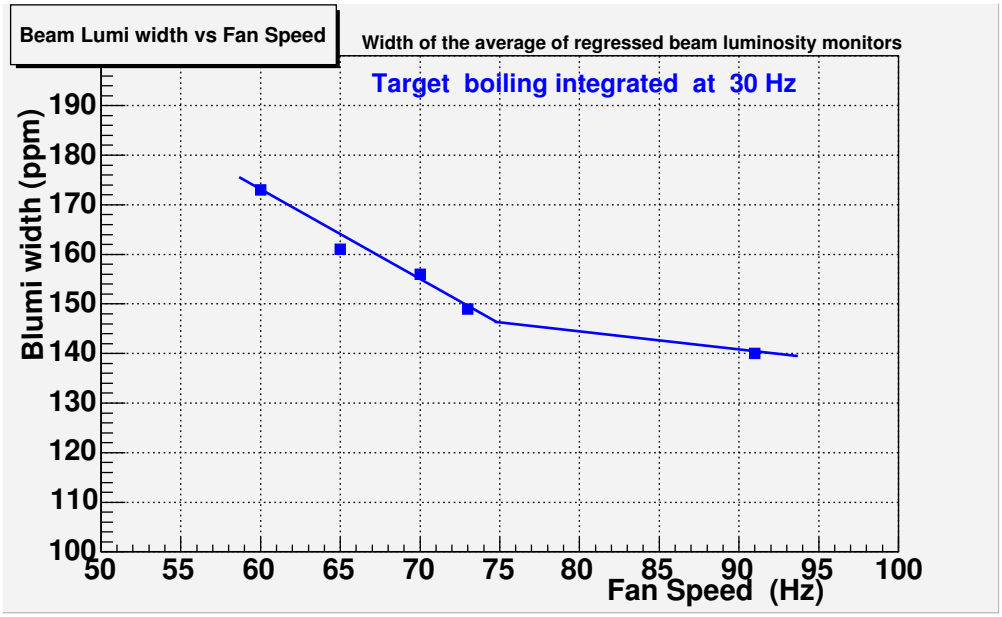

Figure 1: *Hydrogen target density fluctuations; the RMS width (in ppm) of the helicity-pairs measured in the luminosity monitors is shown as a function of fan speed in Hz. Data were taken with 58 μA beam current and 2 mm x 2 mm raster.*

2.3 Møller Polarimeter

The Hall A beam line is equipped with a Møller polarimeter, whose purpose is to measure the polarization of the electron beam delivered to the hall. In 2005, the polarimeter has been upgraded. A new holder has been built and installed. The purpose was to improve the systematic accuracy, associated with the target polarization.

Description	Systematic error	
	old	new
Target polarization	3.5%	2.0%
Target angle	0.5%	0.5%
Analyzing power	0.3%	0.3%
Levchuk effect	0.2%	0.2%
Dead time	0.3%	0.3%
Total	3.6%	2.1%

Table 1: *The most important systematic errors of Møller polarimetry in Hall A, for the old setup and the expectation for the new setup.*

The systematic error is dominated by the error on the target polarization (see Table 1). The target is a magnetized ferromagnetic foil and its electron polarization is measured by measuring the foil magnetization. We found a relatively strong variation of the magnetization results along the foil. In order to treat these variations correctly we are going to measure the relative foil polarization across the foil, using the electron beam. The new target holder provides the target motion across the beam, in two projections. It contains 5 ferromagnetic foils (see Table 2). The foils are stretched on a metal frame (see Fig. 2).

Foil	0	1	2	3	4	5
Material	Al	SM	SM	Fe	Fe	SM
Thickness μm	16.5	13.0	29.4	14.3	9.3	6.8
Origin	-	old	SLAC	Kh	Kh	Kh
$\mathcal{P}_{center}$ % prelim	-	7.95	8.20	7.62	7.42	7.97

Table 2: *The foils installed in the new target holder. The foils dimensions are* 15×3 cm^2*. The foils are made of iron (Fe), supermendur (SM) and one aluminum foil has been installed. The foils were made and annealed at Vacuumschmelze (SLAC) and Kharkov (Kh).*

In 2005, during a period from August 1 till November 1, 7 measurements of the beam polarization have been made. The measurements included scans across the surface of the foils, dependence on the magnetic field and other systematic studies. Preliminary results are presented on Fig. 3. The data analysis is in progress.

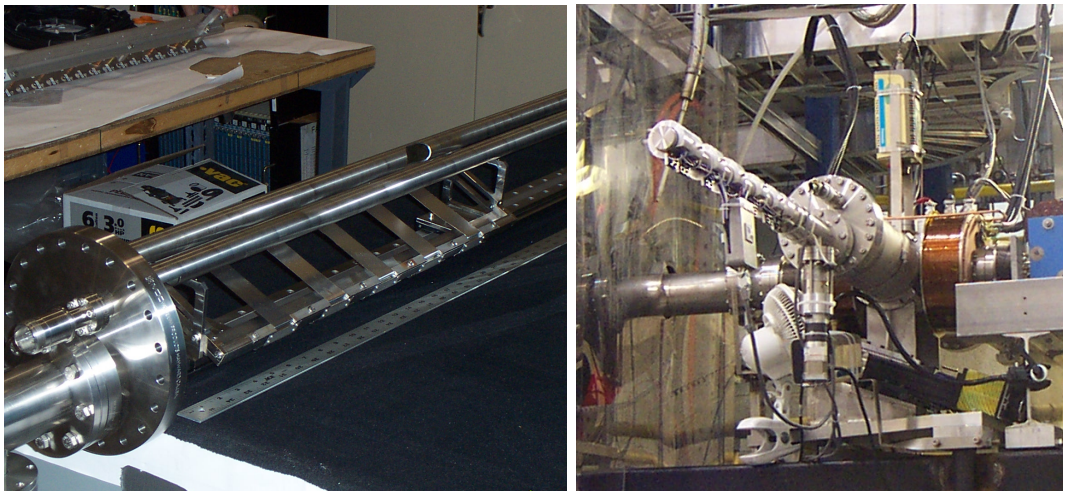

Figure 2: *Left picture: the foils mounting. Right picture: the new target holder installed on the beam line. New Helmholtz coils are installed to provide the required magnetic field at the target area.*

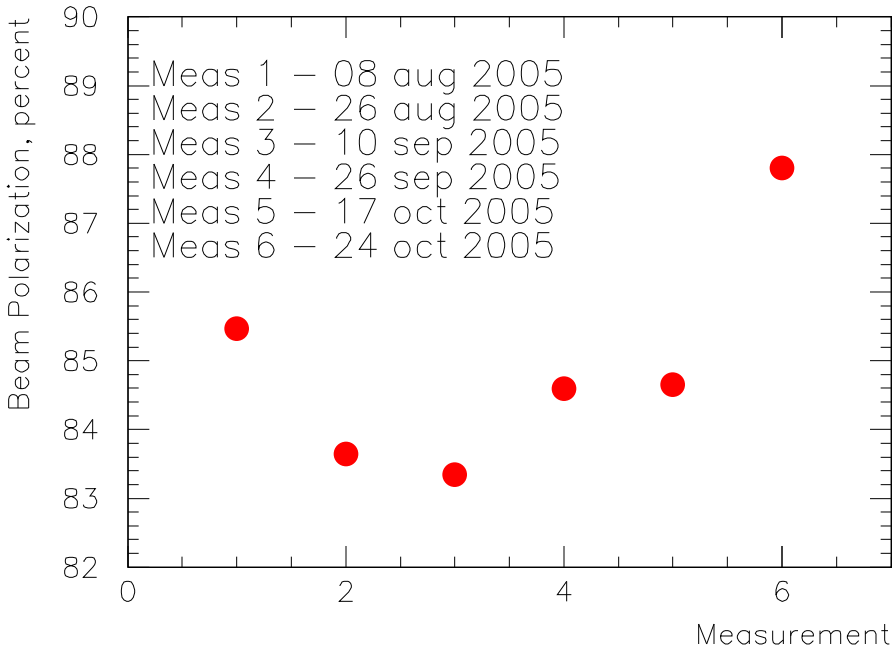

Figure 3: *Preliminary results of 2005, averaged by all targets.*

2.4 BigBite Spectrometer

Contributed by D.W. Higinbotham

2.4.1 Introduction

The BigBite spectrometer has brought a new generation of experiments to Hall A. The first of these, an experiment to investigate short range correlations [2], ran between January 2005 and April 2005. The experiment acquired its proposed data and is currently being analyzed (see Section 3.8). The second BigBite experiment, a measurement of the neutron's electric form factor [3], is scheduled to begin in February 2006. In addition to these experiments, there are four other approved BigBite spectrometer experiments [4, 5, 6, 7] along with one conditionally approved experiment [8].

2.4.2 Magnet

The dipole magnet for the BigBite spectrometer was originally built for the NIKHEF internal target program and was subsequently purchased by Jefferson Lab for use in Hall A. During its first experiment in Hall A, the magnet ran continuously at 518 A (0.92 T) without any problems. This corresponded to the same current as was previously used at NIKHEF and measurements of field at this current agreed with the historic 0.92 T. At the end of the experiment, the magnet was tested to find the maximum current that could be used in Hall A [9]. During this test the BigBite magnet was powered to 890 A which corresponded to a central field of 1.4 T. Unfortunately, after one hour at this setting the magnet's return cooling water temperature was measured to be in excess of 70 C and continuing to rise. Based on the results of the test, the limit for running the BigBite magnet with the present cooling system has been set to 800 A, a little more than 1.2 T, and the BigBite magnet OSP has been updated to reflect this change [10].

2.4.3 Detector Packages

There are already three different detector package configurations for the BigBite spectrometer. The first package, which was built for the short-range correlation experiment [2], is comprised solely of scintillator planes. The first plane, known as the auxiliary plane, is placed immediately after the BigBite magnet. A segmented trigger plane, which is located 1 m further back, is comprised of 3 mm and 30 mm scintillating layers to provide dE/E particle identification and has timing resolution better than 0.5 ns. The auxiliary and trigger planes together provide approximately 5% momentum resolution at 300 MeV/c with approximately 10 mrad angular resolution. The auxiliary plane only has one-sided read-out, so the spectrometer in this configuration is not be able to determine the reaction vertex. In this configuration the BigBite spectrometer has a solid angle acceptance of 96 msr with a vertical acceptance of $\pm$300 mrad and a horizontal acceptance of $\pm$80 mrad.

The second detector package, optimized for detecting low-energy hadrons, uses the same trigger plane but the auxiliary plane is replaced by two drift chambers. The chambers allow BigBite to provide approximately 1% momentum resolution, 3 mrad

angular resolution in θ and ϕ, and 3 mm y-target resolution. This package will be used for measurements of threshold pion production [5], and detailed measurements of the ^{3}He system [4]. As with the previous setup, in this configuration the BigBite spectrometer has a solid angle acceptance of 96 msr.

The third detector package is being optimized for detecting high-energy electrons and will be used for the G_E^n, Pentaquark, and transversity experiments [3, 6, 7]. This package uses three drift chambers to give the spectrometer its best possible multi-track capability. In addition to the drift chambers and a trigger scintillator plane, this package also has a preshower and shower calorimeter system. Due to the fact that the detector package much be lowered to optimally detect high energy electrons, in this configuration the spectrometer has a 75 mrs solid angle acceptance.

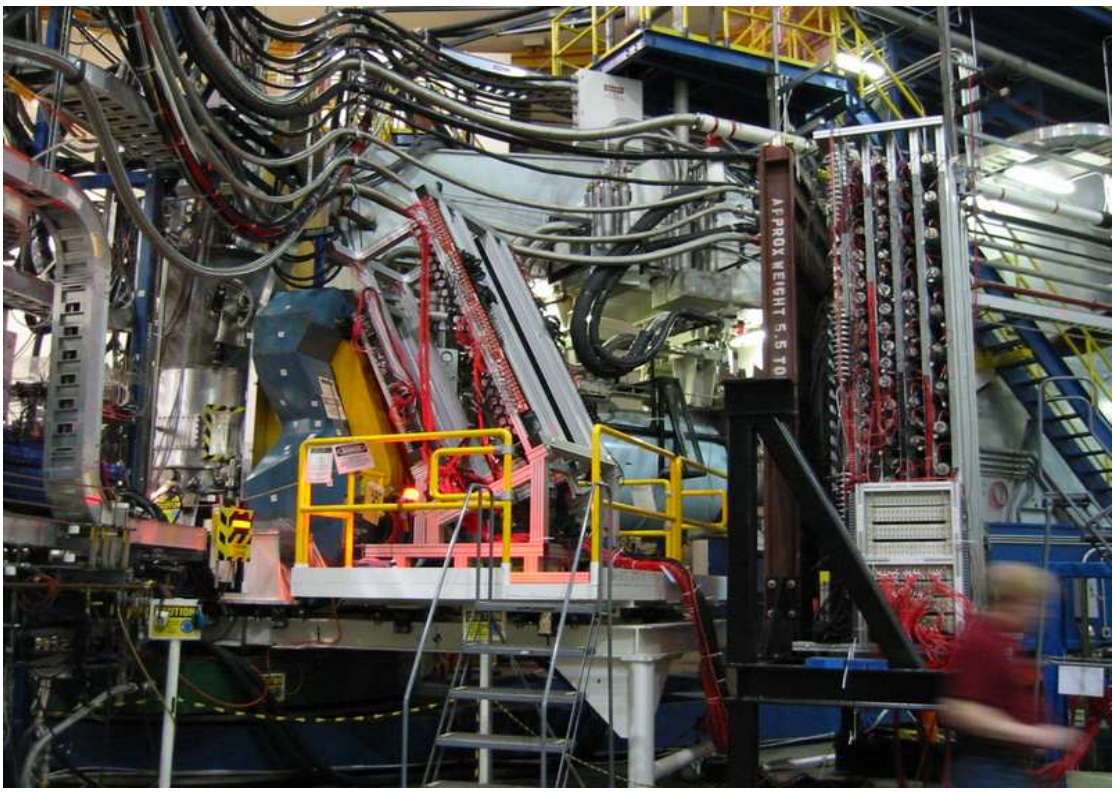

Figure 4: Shown is a photo of the short-range correlation experiment's equipment as installed in Hall A. Located left of center is a new scattering chamber which matches BigBite's large out-of-plane acceptance and which turned out to be very useful for accessing the target area during the subsequent HAPPAEX II hydrogen and helium experiments. The BigBite dipole magnet is located right of the chamber with the auxiliary and trigger planes located behind.

2.4.4 Summary

A flexible, large-acceptance spectrometer has been built for Hall A. The first BigBite experiment, the short-range correlation experiment, was successfully completed in April 2005. The second BigBite experiment will be the G_E^n experiment which is scheduled to begin in late February 2006. With many other new and approved experiments, the BigBite spectrometer has become a key component of the Hall A physics program.

2.5 Podd — C++/ROOT Analysis Software

Contributed by J.-O. Hansen

After the successful introduction last year of the new C++/ROOT-based analysis software package Podd, the Hall A analysis software has entered a rather stable maintenance mode. All production experiments that ran in 2005 used Podd for their online and offline data analysis (except for HAPPEX-2, which has special requirements and therefore employed custom software).

The core part of Podd continued to be improved throughout the year. Several updates were made to the decoder, including support for new hardware for the BigBite spectrometer and the upcoming G_E^n experiment. The writing of ROOT objects (*e.g.* `TLorentzVector`) to the output is now supported for any detector and physics module class. The scaler classes have been restructured and use a more intelligent database layout. χ^2 calculations were added to the track-fitting routines, and various additional kinematical quantities are now calculated by the physics modules. Support for 64-bit platforms and ROOT 5 was added. Finally, a number of minor bugs were corrected, and some usage inconveniences were improved on.

During the summer of this year, we built on the existing Monte Carlo input interface, using a custom "decoder", to carry out a study of the VDC track reconstruction performance. As a first result, a number of minor bugs in the VDC code (ambiguous database information) were found in this way. In the actual study, the tracking performance was found to be surprisingly good even in the presence of multiple tracks. However, we also found a surprisingly strong sensitivity to random noise in the chambers. Complete details can be found in a Tech Note [19]. The study made it obvious that the VDC tracking performance can be improved with a more intelligent, noise-filtering algorithm. These improvements will be implemented as time permits.

The documentation of the software is still incomplete and will receive highest priority in 2006. In addition, there are plans to re-write the decoder package in a truly object-oriented fashion to simplify the addition of new hardware. Finally, the database system has been found to have certain inconvenient limitations, which will be addressed in the longer term.

The work reported here was carried out in collaboration with R. Feuerbach, R. Michaels, and B. Reitz from Hall A. Our summer student, Amy Orsborn, did a marvellous job with the VDC simulation studies.

2.6 High Resolution Spectrometer Optics

Contributed by D.W. Higinbotham

2.6.1 Overview

The Hall A High Resolution Spectrometers (HRS) were designed to have a momentum resolution of 1×10^{-4} full width at half maximum (FWHM). The best direct measurement of the momentum resolution, the ^{12}C(e,e$'$) elastic scattering data shown in the Hall A NIM paper [12], has a FWHM of 2.5×10^{-4}. The difference between the design value and the measured value has been calculated to be due to multiple Coulomb scattering in the various materials that were between the carbon target and the spectrometers' wire chambers. The measurement was also done with a beam energy energy of 845 MeV at an angle of 16°; thus the scattered electrons only had a momentum of 842.5 MeV/c. This relatively low momentum enhanced the effect of multiple Coulomb scattering which is promotional to $\frac{1}{p}$ for relativistic electrons. Recently, we had the opportunity to repeat the carbon elastic measurement with a setup that would minimize the effect of Coulomb scattering and allow for a direct determination of the momentum resolution of the HRS.

2.6.2 New Calibration

During the Hall A Hypernuclear experiment [20], the HRS were vacuum coupled to the scattering chamber, dramatically reducing the material between the target and the wire chambers. Furthermore, the measurement was made with a beam energy of 1852 MeV and a scattering angle of 6°, resulting in a scattered electron momentum of 1850 MeV/c for carbon. Thus reducing the effects multiple Coulomb scattering even further.

For the new optics calibration, elastic data was taken not only with two different thickness of carbon, 100 mg/cm^2 and 10 mg/cm^2; but also, with a 100 mg/cm^2 tantalum target. Due to tantalum's significantly heavier mass, it has relatively little recoil as compared to carbon, making it an excellent choice for calibration. The difference in the recoil of carbon and tantalum is illustrated in Fig. 5 with a scatter plot of the analyzer variable L.gold.dp, dp/p, versus the L.gold.ph variable, which corresponds primarily to the scattering angle. This effect can be calculated using the kinematic relation

$$E' = \frac{E}{1 + \frac{2E'}{M} sin^2(\frac{\theta}{2})}, \tag{1}$$

where E is the energy of the beam, E' is the energy of the scattered electron, M is the mass of the target nuclei, and θ is the scattering angle. When using carbon one needs to correct for the correlation between the angle and dp/p; while for target as masses as tantalum, this correction is practically zero and any error due to angle uncertainties is also becomes practically null. The data shown in the Fig. 5 was taken without changing any spectrometer or beam parameters.

2.6.3 Results

For determining the new optics matrix elements, only tantalum elastic data was used; eight different momentum settings were combined in order to cover the momentum

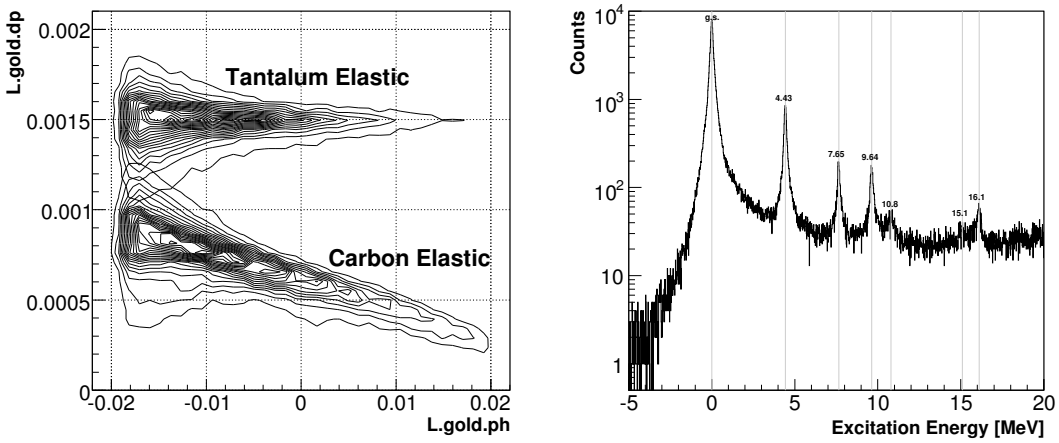

Figure 5: *Shown in the left panel is a contour plot of carbon and tantalum elastic scattering data where the difference in the slopes is due to the difference in the nuclear masses. Shown in the right panel is the kinematically corrected carbon elastic data using the matrix elements obtained using the tantalum elastic data. The carbon ground state peak along with the indicated inelastic peaks each have a FWHM of less than 200 keV. This width translates to a dp/p resolution of less than* 1×10^{-4}.

acceptance of the spectrometers. For each momentum setting, the data was broken into a L.gold.ph greater than zero and a L.gold.ph less than zero block. This allowed the optimization code to balance the amount of small scattering angle data with the amount of the slower counting larger angle data. Once the matrix elements were optimized, the carbon elastic data was used to check the quality of the matrix elements. As the carbon inelastic states cover over 1% of the focal plane, this turned out to be a rather stringent test Doug, this sentence is not clear. In Fig. 5, the kinematically corrected carbon excitation spectrum is shown. During all of these measurements, the accelerator division took great care to maintain both a beam energy spread and the absolute beam energy to a FWHM of better than 1×10^{-4}. The final result was a FWHM for each of the elastic and inelastic peaks in the carbon elastic data of 1×10^{-4}, demonstrating the design momentum resolution specification of the two spectrometers.

2.7 Status Report on the Polarized ^{3}He Target

(Contributed by J. P. Chen)

The Hall A polarized ^{3}He target [23] was successfully used in it's standard configuration for the experiments E94-010 [24] and E95-001 [25], E99-117 [26], E97-103 [27], E01-012 [28] and E97-110 [29].

The standard polarized ^{3}He target used optically pumped Rubidium vapor to polarize ^{3}He nuclei via spin exchange. Two sets of Helmholtz coils provided a 25 Gauss holding field for any direction in the scattering (horizontal) plane. Target cells were up to 40 cm long with density of about 10 amg (10 atm at 0°). Beam currents on target ranged from 10 to 15 μA to keep the beam depolarization effect small and the cell survival time reasonably long ($>$ 3 weeks). The luminosity was about 10^{36} nuclei/s/cm^2. The in-beam average target polarization achieved was typically over 40%. Two kinds of polarimetry, NMR and EPR (Electron-Paramagnetic-Resonance), were used to measure the polarization of the target. The uncertainty achieved for each method was less than 4% relative and the methods agreed well within errors.

The next polarized ^{3}He experiment, (E02-013,G_E^n [30]), will operate the target very close to the BigBite spectrometer. To minimize the fringe field effect from the BigBite, a new magnet with an iron box to shield the BigBite field has been constructed. The design work and construction for a new mechanical system with a redesigned target ladder, motion and support system, oven, RF coils and pickup coils has been mostly completed. The new oven is needed to accommodate higher temperature (of 230° C) for target cells that use K-Rb hybrid spin-exchange technique [31]. Due to the much higher K-^{3}He spin exchange efficiency, the new hybrid cells have significantly shorter spin-up times and improved performance . There are about eight usable hybrid cells manufactured by the UVa (Gordon Cate's) group and the William and Mary (Todd Averett's) group, Most of the cells have spin-up times of 6-8 hours and polarizations of 40-50 hours.

A new laser building next to the counting house was constructed earlier this year to replace the laser hut in the hall. A new target lab with its infrastructure and safety interlock system has been setup in the new laser building. The G_E^n target system has been setup and is being tested in the new target lab.

With the laser building moved outside the hall, a optical fiber system is needed to transport the laser light into the hall. Eight 75m-long optical fibers and two 5-to-1 combiners were purchased and tested. The typical light intensity drop through the optical fiber system is about 15%. Air cooling and a temperature interlock system are used to protect the fibers from over-heating.

A new NMR system has been setup and is under testing. Both RF sweep and field sweep have been tested. Water calibration for RF sweep has significant RF background and improvement is needed before it reaches usable stage. Field sweep has been improved to accommodate the hysteresis effect due to the iron box. A new EPR system has been setup. Initial tests were successful, and extensive tests are underway.

R&D study for single target spin asymmetry experiments (E03-004 [32] and E05-015 [33]) is underway. Modifications are being developed to have fast spin-reversal. The target spin will be flipped with RF AFP technique and the laser polarization flip will be accomplished with rotating quarter-wave plates.

2.8 Hall A RICH Detector

Contributed by E. Cisbani and B. Reitz

The Hall A Proximity Focusing RICH, which has been described in previous annual reports, has been installed in the HRS-Left and successfully operated during experiment E94-107 "Hypernuclear Spectroscopy" in June and July 2005. The RICH performed slightly better than during the first part of experiment E94-107 and E04-012, which were running in 2004 [11]. The rejection factor and kaon detection efficiency have been improved and together with the good performances of the renewed aerogel Cherenkov counters [12] a remarkable kaon separation has been obtained.

2.8.1 Maintenance

When the chamber of the RICH is not flashed with clean and dry gas for an extended period of time, the hygroscopic CsI layer (300 nm), which is evaporated on the pad plane, degrades. In this case first a cleaning of the pad plane and then a new evaporation of CsI is required.. This procedure has been performed in May 2005 before the installation of the RICH into the left HRS. All three pad planes forming the RICH photon detector chamber have been cleaned and re-evaporated. The quality of the evaporation has been estimated by the on-line quantum efficiency measurement whose result, for the first pad plane is shown in Fig. 6.

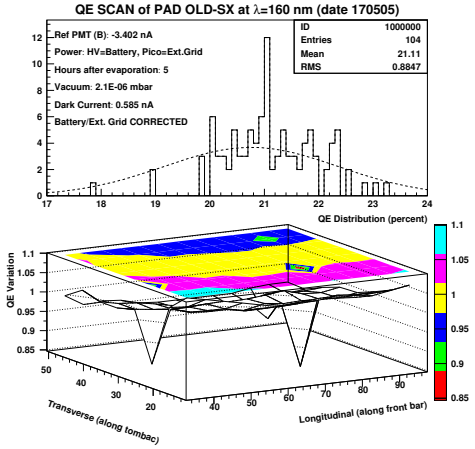

Figure 6: Quantum Efficiency of the first pad plane, evaporated in May 2005. Similar results have been obtained with the successive evaporations of the second and third pad plane.

During the installation of the RICH detector in the detector stack of the left HRS, the radiator - a vessel containing the liquid freon - was severely damaged and developed a leak of freon into the wire chamber. Subsequently the radiator was replaced by a spare radiator, after the latter was reinforced to avoid future problems of this kind.

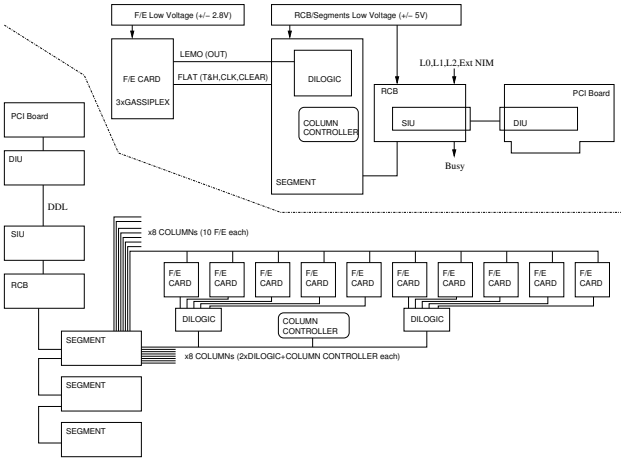

Figure 7: New electronics scheme.

2.8.2 Data Analysis

The PID algorithm has been improved using a more sophisticated estimate of the centroid of hits (and therefore of the optical photon impact point) by means of a fit with the Mathieson distribution. The analysis of the RICH misalignment effects is underway.

2.8.3 Upgrade

The Hall A RICH detector and its front-end electronics as used during experiment E94-107 where limiting the maximum readout rate of the DAQ system in Hall A. In order to increase the readout rate, a new front-end and readout electronics has been adapted from the ALICE RICH HMPID [13]. The new electronics offer, at a competitive price, improved speed, high modularity, and relative compactness. It is based on a new version of Gassiplex front end cards and a multiplexing/ADC stage based on the fast (up to 40 MHz) DILOGIC chips, which are controlled by programmable FPGAs. The schematic setup is shown in Fig. 7. The column boards (containing the DILOGIC chips) are connected via a customized backplane to a segment. Segments are readout in series and controlled by a RCB (readout controller board) card. This customized front-end electronics are connected via a DDL link, a optical link capable of high transfer rates (2 GigaByte/sec), to a dedicated DAQ computer.

The a full set of the new electronics is available at JLab, and currently under testing. It is expected to double the present acquisition rate limit imposed by the VME based CRAMS/Sequencer modules.

The Hall A RICH detector was designed and optimized for particles with momenta around 2 GeV/c. In the perspective of extending the momentum range of the identifiable particles to 3 GeV/c and above a couple of solutions have been investigated by GEANT3 based MonteCarlo simulation:

1. replace the actual radiator C_6F_{14} by C_5F_{12} liquid freon which has a lower (1.24) refractive index.

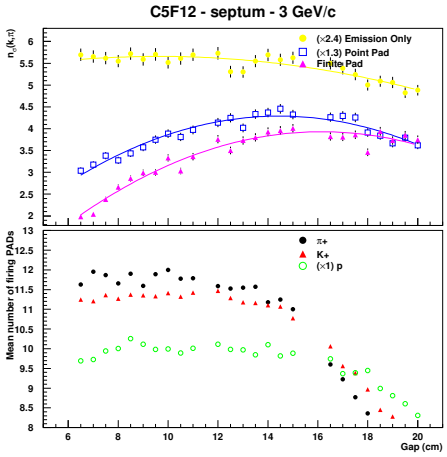

Figure 8: MonteCarlo simulation of the improved RICH (normalized to the real data of the existing RICH); top: angular separation of the $\pi-$K distribution as a function of the gap distance for three different levels of model approximations. Bottom: mean number of hits.

2. increase the proximity gap of few centimeters using a frame spacer.

The main results are summarized in Fig. 8, which shows that using a radiator with an refractive index of 1.24 and a proximity gap of 14-16 cm, the separation between the kaon and pion angular distribution is at the level of 3.5 sigma for particle momenta of 3 GeV/c.

2.9 Pressurized Čerenkov for Hall A

Contributed by Robert J. Feuerbach

2.9.1 Motivation

The upcoming Transversity (E03-004) and Pentaquark (E05-009) experiments require kaon identification for momenta in the range of 2.3 to 3.1 GeV/c. While the existing RICH detector can perform in this region, its ability to differentiate between particle types decreases for higher momentum, it does not handle high singles rates well, cannot be maintained easily with on-site resources, and does not provide a trigger-level signal for event selection. In order to simplify particle identification, primarily pion/kaon separation, at momenta above 2 GeV/c a Čerenkov detector is being designed which utilizes the present Gas Čerenkov detector's proven optics in a manner where the threshold momentum for pions is in the 2 GeV/c region. This is achieved through the use of C_4F_{10} as a radiator at a pressure of 10 psig.

2.9.2 Design considerations

The original gas Čerenkov detectors built by Saclay and INFN [21] have served Hall A well, providing 7 (12) photoelectrons per electron with a radiator depth of 80cm (130cm) to separate electrons from a pionic background. To it use for pion/kaon separation, a radiator with a larger index of refraction is necessary. The gas we have chosen is C_4F_{10} due to its high index of refraction as well as its benign environmental properties. By using C_4F_{10} as the radiator (see Figure 9) the threshold momentum for pions can be set in the region of 2 to 3 GeV/c, permitting for a direct method to separate pions from kaons 4 GeV/c. To increase the photo-electron yield and reduce the threshold momentum, the gas would be pressurized to approximately 1.7atm (10.3psig).

To accommodate the increased internal pressure, the structure of the Čerenkov would be changed. The modified box would include new thin 0.38mm titanium entrance and exit windows, sealed photomultiplier-tube housings such that the PMTs could be serviced while the detector is pressurized, and modifications to the gas manifolds. The mirrors and relative photomultiplier-tube placement would remain unchanged, so ten three-inch PMTs would be used to collect the photons. A finite element analysis (FEA) of the present detector has been performed to evaluate and plan the necessary structural changes.

The PMT housings have been designed with help from the Argonne group. The main feature is a 1cm Fused silica window [22] to seal the PMT from the pressurized interior of the detector. The material was chosen for its high transmitivity of UV-photons ($\lambda > 200$nm) to preserve the option of adding a wave-shifter coating to the PMT windows. A large concentration of He inside Hall A has been observed in the past, which can dramatically reduce PMT life time. To mitigate this, the housing is also loosely sealed to the hall's atmosphere and flushed with air pumped from outside.

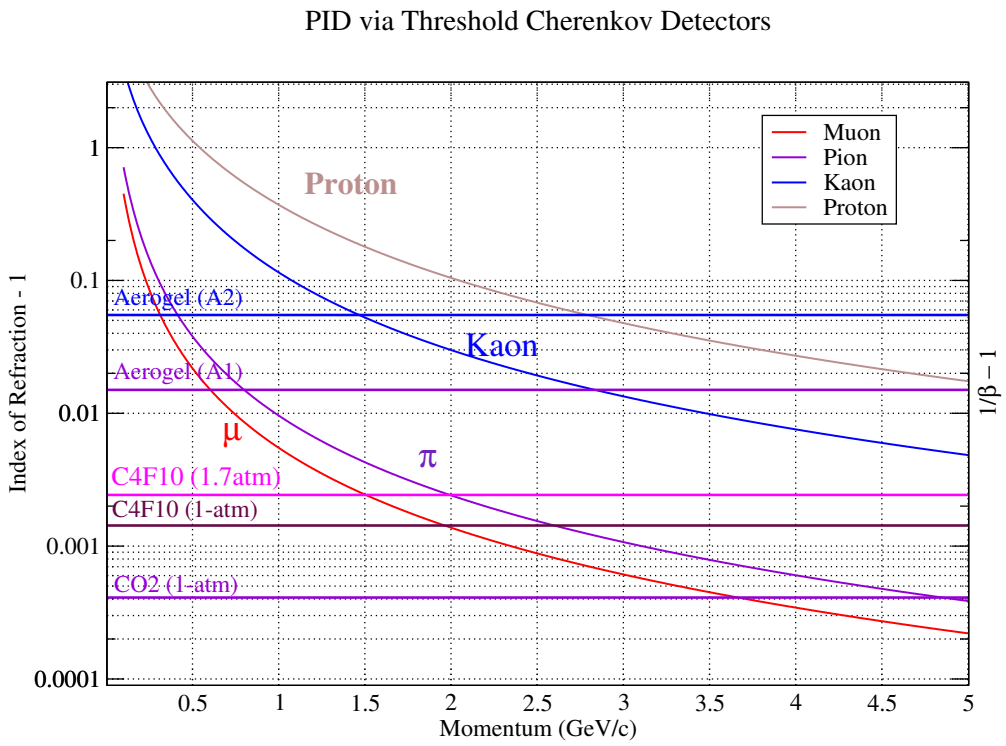

Figure 9: *PID for Threshold Čerenkov Detectors* For each particle type, $\beta^{-1} - 1$ is plotted versus momentum, to be compared to $n - 1$ where n is the index of refraction of a material.

2.9.3 Anticipated Performance

The performance of the Čerenkov detector can be estimated by scaling the present performance of the 80cm deep CO_2 Čerenkov to account for the changed different index of refraction. The pressurized Čerenkov detector is predicted to produce ten photo-electrons for a 2.3 GeV/c pion (see Figure 10), sufficient for a pion rejection factor of 400 or greater for a cutoff of 2 photo-electrons. In addition, the detector could continue to be used for pion/electron discrimination. The entrance windows contribute additional delta-electrons, an additional $4 * 10^{-4}$ for a 4.4 GeV/c pion, but the detector could be run pressurized and filled with CO_2 to increase the photon yield and achieve the same pion/electron separation of the long Čerenkov within a smaller space.

2.9.4 Acknowledgments

It is a pleasure to thank B. Wojtsekhowski for the original concept of the pressurized Čerenkov, P. Brindza for evaluating the different window designs, R. Anumagalla for the extensive finite element analysis of the detector, and T. O'Connor of Argonne National Laboratory for the final design of the PMT housings.

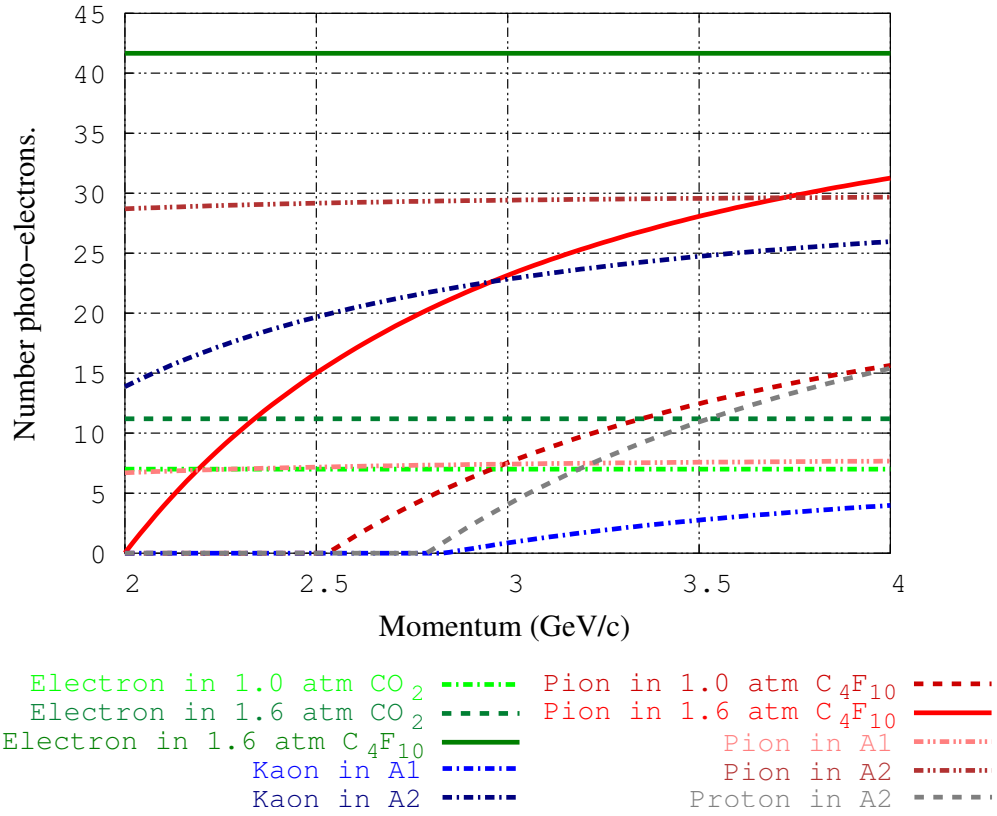

Figure 10: *Number of collected Photo-electrons* The anticipated number of collected photo-electrons for different particles and radiators as a function of momentum. The depth of the radiator is 80cm, and the results are scaled from the present performance of the atmospheric-pressure CO_2 radiator for electrons (shown as the light-green dot-dashed line).

3 Summaries of Experimental Activities

3.1 E94-107: High-resolution hypernuclear 1p shell spectroscopy

Contributed by Franco Garibaldi, for the Hall A kaon collaboration

3.1.1 Introduction

Experiment E94-107 at Jefferson Lab is designed to perform high resolution hypernuclear spectroscopy by electroproduction of strangeness on 1p-shell targets: ^{12}C, ^{9}Be, ^{16}O.

Hypernuclear spectroscopy provides fundamental information needed to understand the effective Lambda-Nucleon interaction. Experiments up to now have been carried out essentially by means of hadron-induced reactions, capable of limited energy resolution (about 1.5 MeV at best). Such studies yielded information only on the central part of the potential because of the limited spin flip transition terms. In the electromagnetic case, on the contrary, the spin flip transition terms dominate. In addition, the reaction takes place on the proton, while it occurs on the neutron with hadron probes (K^- and π^-). Therefore, using electromagnetic production, *new* hypernuclei are created. An experiment on a ^{12}C target was previously performed with electrons in Hall C, showing the feasibility.

The first part of the experiment on ^{12}C and ^{9}Be targets was performed in January and April-May 2004 in the experimental Hall A. The second part of the experiment (^{16}O) was carried out in June 2005.

Two septum magnets and a Ring Imaging Cherenkov detector (RICH) were added to the existing Hall A apparatus, to have reasonable counting rates and excellent particle identification respectively, as required for the experiment. The new experimental devices (septum magnets and RICH detector) have been proven to be very effective. The RICH detector provided excellent kaon identification and a clean kaon signal over a large pion and proton background.

The physics motivation, the experimental challenges and the needed improvements on the Hall A apparatus (septum magnets, aerogel detectors, RICH detectors, waterfall target) were described in the previous Hall A report. The RICH detector performance is described elsewhere in this report.

3.1.2 ^{12}C and ^{9}Be analysis

The physics information that can be extracted from the data depends also on the energy resolution. For this reason the analysis has recently been focused mainly on the optics data base and on the raster correction. Moreover the evaluation of the efficiency of the different detectors is underway to allow to evaluate the absolute cross section. Fig. 1 shows the effect of the RICH detector on the missing mass spectrum. Two peaks emerge clearly out of background, in the core excited part of the spectrum, at energies 2.5 MeV and 6 MeV when the RICH cuts are applied. The data looks very good compared with the published data obtained both with hadron and electron induced reactions. In order to improve the optics data base, new elastic data on ^{12}C have been taken in June (see the contribution on HRS optics by D. W. Higinbotham). Using this new optics data, a consequent improvement in the missing mass spectrum has been obtained. Nevertheless

the expected missing mass resolution (600 KeV) has not been achieved yet. Work is underway to understand and correct the beam parameters, energy beam stability, position beam stability, raster correction (for ^9Be) etc.

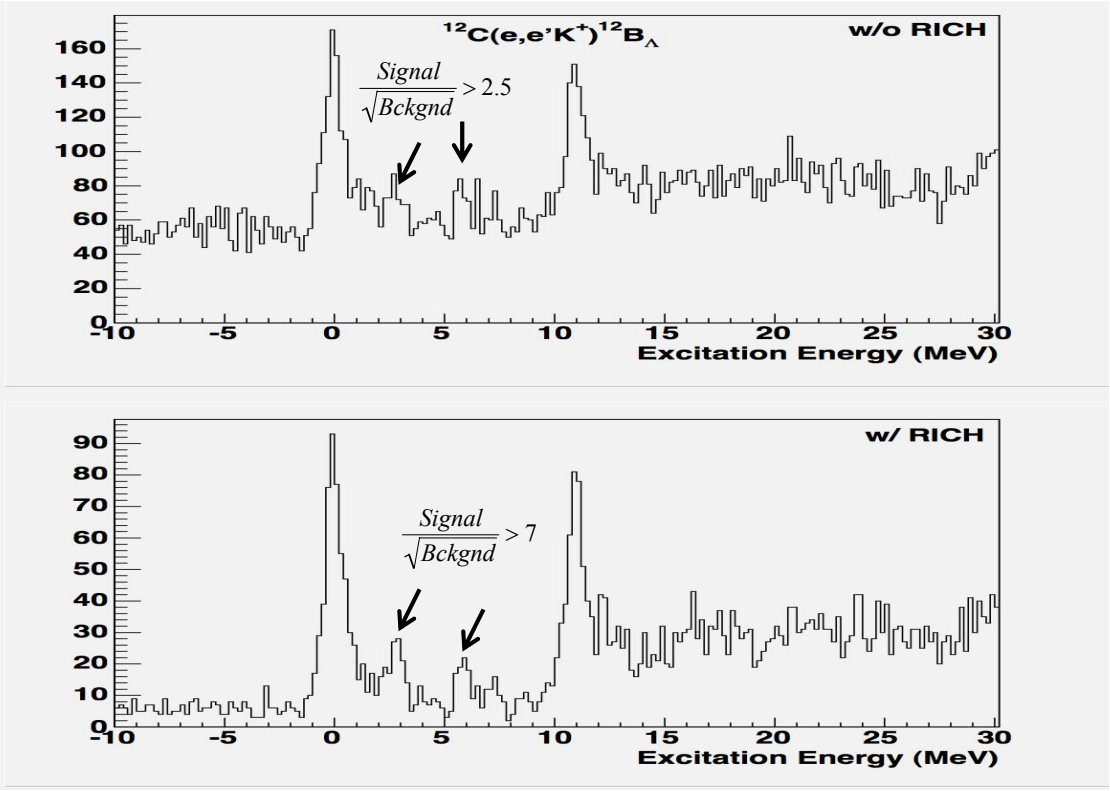

Figure 11: ^{12}C missing mass spectrum with and without RICH cuts.

3.1.3 ^{16}O analysis

The reasons for studying such a nucleus are different. Information about an upper limit on doublet splitting of first excited J=1,2 doublet at $\sim$ 7 MeV can be obtained in principle. Moreover from the energy spectra of the mirror hypernuclei $^4H_\Lambda$ and $^4He-\Lambda$ it has been deduced that that the hyperon-nucleon interaction contains a non-negligible charge-symmetry-breaking part. Therefore it is extremely interesting to study other pairs of mirror hypernuclei, to compare their energy spectra and thus look for some additional evidence of these effects. $^{16}O_\Lambda$, well known from meson hypernuclear production, and $^{16}N_\Lambda$, reachable in electroproduction, are good candidates. Moreover using the waterfall target allows the study of the elementary reaction in a kinematical region where data are absent. In fact we are close to the photon point, so data can be compared with the CLAS and SAPHIRE data that show some inconsistency among them. The kinematics, the counting rates and the main beam parameters are reported in the Table.1.

Here we report the results of a very preliminary analysis. In Fig. 2 (a,b) we report

E_{beam} (GeV)	P_e (GeV/c)	$q_e = q_K$ (GeV/c)	ω (GeV)	I (μA)	Q^2 (GeV/c)^2	Target thickness (mg/cm^2)	Counts (/peak/hr)
3.656	1.44	6	2.2	100	0.079	$\approx$ 100	$\approx$ 0.1 - 10

Table 3: The kinematics, counting rates and the main beam parameters

Hyperneucleus	B_Λ (MeV)
$^4He_\Lambda$	2.39
$^4H_\Lambda$	2.04
Δ_{CSB}	0.35
$^{12}B_\Lambda$	11.37
$^{12}C_\Lambda$	10.0
Δ_{CSB}	0.57
$^{16}N_\Lambda$	13.6 $\pm$ 0.1 ?
$^{16}O_\Lambda$	13.0
Δ_{CSB}	0.6 $\pm$ 0.1

Table 4: Binding energy and charge symmetry breaking for different nuclei

the hydrogen and the oxygen missing mass spectra obtained by the interaction of electrons with the waterfall target. On such a target besides the main goal of measuring spectroscopy on the 16N$_\Lambda$ hypernucleus, the cross section of the exclusive elementary process of KΛ electroproduction off protons, p(e,e$'$K)Λ can be measured as well. The kinematics under study, at a Q^2 value as low as $Q^2 2 = 0.079$ (GeV/c)^2, and with the kaon produced in the very forward direction with respect to the virtual photon is of particular interest. In such a region the photon is almost real and these data can be compared with existing photoproduction data which show inconsistent measurements among different collaborations. CLAS and SAPHIR data sets for example do not agree, especially at small ?K? angles, where our cross section can be measured. The experimental situation can be thus clarified and theoretical models can be better constrained.

Fig. 12 shows the Oxygen missing mass spectrum compared with a theoretical prediction. Four peaks are clearly visible in the missing mass spectrum (g.s., $\sim$7 MeV, $\sim$12 MeV, $\sim$18 MeV). The same happens in the data from a hadron induced hypernuclear production experiment (see Fig. 12) [**?**] (T. Takahashi et al, Nucl. Physics A760 (2000) 265c).

Fig. 12 shows the $^{16}N_\Lambda$ missing mass spectrum compared with a theoretical model. The Saclay-Lyon (SLA) model has been used for the elementary K$^+$ - Λ production. The hypernuclear wave function has been computed by M. Sotona. The curve has been normalized to the ground state peak. It seems that the high energy excited multiplet is not well reproduced. One has to consider that we are in the p Λ-shell where the Λ-N interaction is poorly known. Fig. 6 shows that a very good agreement is obtained if one shifts *by hand* the position of the multiplet in the model, while maintaining the predicted strength. Work is going on for better understanding of this required shift.

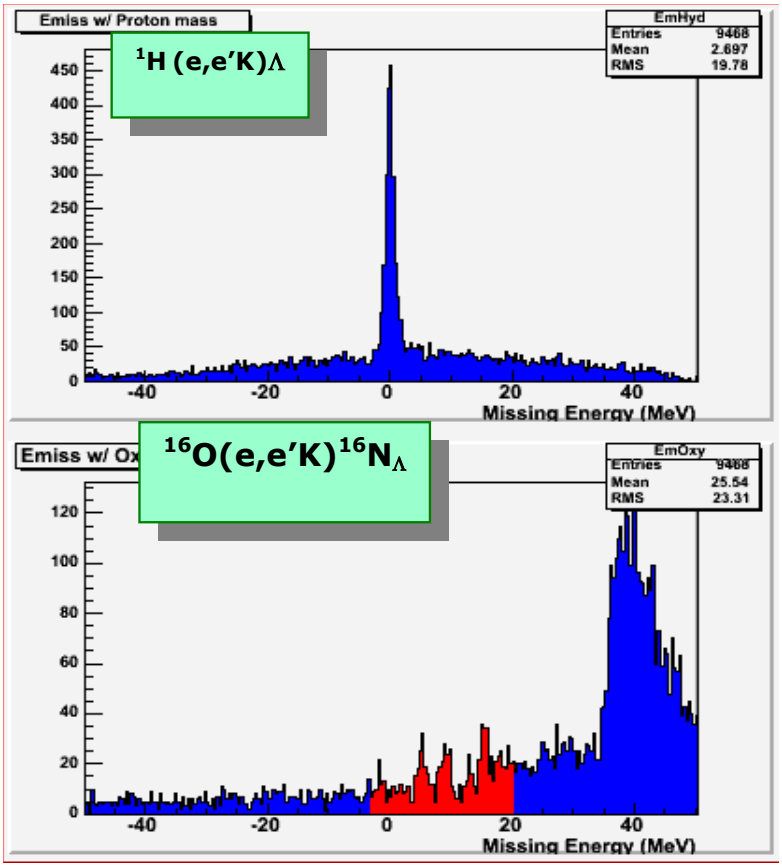

Figure 12: The missing mass spectra of hydrogen and Oxygen from the waterfall target

Λ binding energy in $16\mathrm{N}_\Lambda$ is estimated (very preliminary!) to be $\mathrm{B}_\Lambda(^{16}\mathrm{N}_\Lambda) \sim 13.6$ MeV and charge symmetry breaking for these *doublets* of known mirror hypernuclei are shown in Tab. 2

3.1.4 Conclusions

The goal of the Experiment E94-107 is to carry out a systematic study of light hypernuclei (p-shell). The experiment required important modifications of the Hall A apparatus. Good quality data on ^{12}C and ^{9}Be targets ($^{12}\mathrm{B}_\Lambda$ and $^{9}\mathrm{Li}_\Lambda$ hypernuclei) have been taken last year. New experimental equipments showed excellent performance. The RICH detector performs as expected and it is crucial in the kaon selection. On-going analysis of data on ^{12}C target is showing new information on $^{12}\mathrm{B}_\Lambda$ and interesting comparison with theory for $^{12}\mathrm{B}_\Lambda$ and $^{9}\mathrm{Li}_\Lambda$. Very promising physics is coming out from new data on the waterfall target for $^{16}\mathrm{N}_\Lambda$ hypernuclear spectroscopy - also for the p(e,e′K)Λ cross-section measurement.

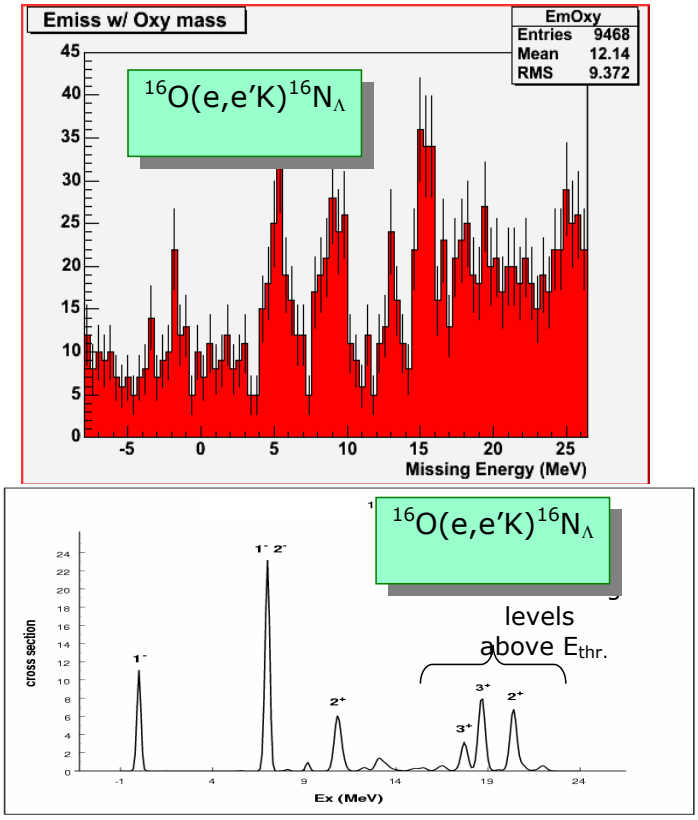

Figure 13: 16N spectrum compared with a theoretical prediction

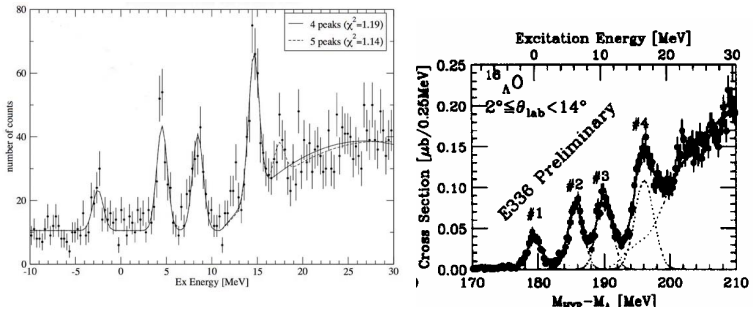

Figure 14: Oxygen missing mass spectrum from our experiment ($^{16}N_\Lambda$) and oxygen missing mass spectrum obtained with hadron probe ($^{16}O_\Lambda$). Four peaks are clearly visible in both cases.

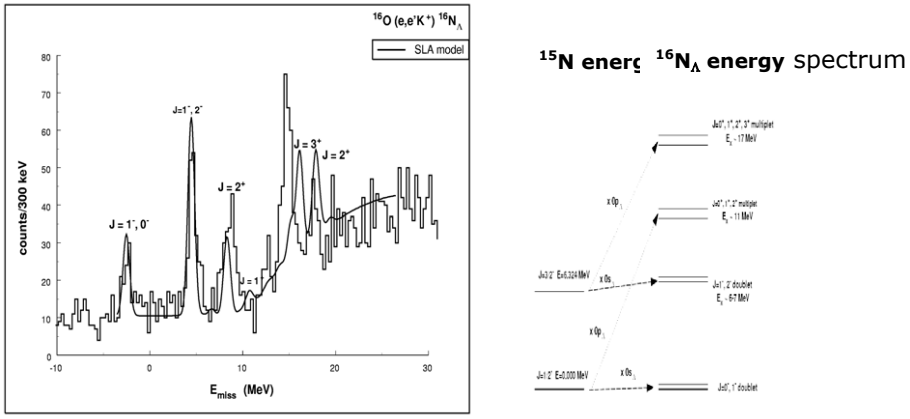

Figure 15: Comparison with a theoretical model

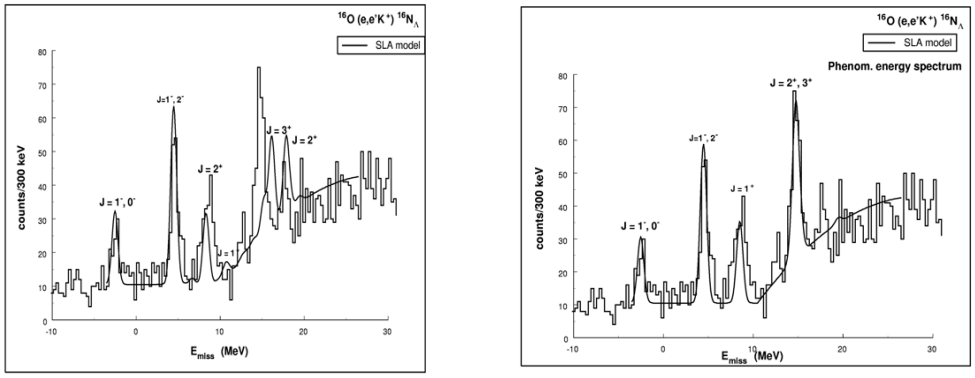

Figure 16: Shifting *by hand* the position of the multiplet a good agreement is obtained

3.2 E97-110

Progress report on E97-110: The GDH Sum Rule, the Spin Structure of ^{3}He and the Neutron using Nearly Real Photons

J.-P. Chen, A. Deur, F. Garibaldi spokespersons
and
the E97-110 Collaboration.

The goal of the experiment is to measure the generalized Gerasimov-Drell-Hearn integral (GDH) and moments of spin structure functions at low Q^2 on the neutron and ^{3}He. A brief description of the physics goal and of the running of the experiment was given in the 2003 Hall A report.

The experiment The experiment ran in April-May and July-August 2003. The first part of the experiment (low Q^2, April-May 2003) acquired data with a mis-wired septum magnet. The septum was fixed in June and the experiment was completed in July-August.

Present state and outlook Data analysis efforts have been concentrated on the second period which contains the bulk of the data and is easier to analyze:

The optic study of the spectrometer-septum combination is completed (V. Sulkosky, Col. of William and Mary). The acceptance study and SNAKE-modeling of the magnetic transport for 6^o is nearly completed (V. Sulkosky), see figure 17. It will be tested using data from kinematics of known cross sections. The same analysis will be carried out for 9 degrees. Particle Identification (PID) analysis, which comprises the calibration of preshower and shower detectors and Cerenkov counters, and PID efficiency analysis, is completed (H. Lu et al, USTC: University of Science and Technology of China). A parallel analysis is being finalized (J. Yuan, Rutgers). The VDC analysis is underway (S. Dhamija, U. of Kentucky). The remaining task being to develop an algorithm to deal with multitrack events for the high rate settings. The nitrogen analysis that will determine the dilution of the ^{3}He asymmetry is underway (X. Zhan, MIT). Beam characterization for the two run periods is being finalized (T. Holmstrom, Col. of William and Mary). The C++ analyzer was adapted for the experiment and batch analysis codes are available (V. Sulkosky). A final database recording the characteristics and quality of runs is being established for both first and second periods (J. Singh, UVa).

The data analysis for the first period is also under way. The study of the optics and acceptance for the spectrometer/mis-wired septum combination is near completion (N. Liyanage, UVa). The remaining task is to test the procedure with elastic data and other kinematics of known cross sections. The shower and Cerenkov calibrations are underway (H. Lu et al). A GEANT4 simulation is being developed (A. Beck, MIT). It will be used to study target collimator punch-through and "two-step process" backgrounds. It was shown using a simpler simulation that these effects need to be studied precisely for the first run period, see the 2004 report. The background is smaller for the second run period and the simpler simulation is enough to correct for it.

Near term plan includes completion of the acceptance study and other tasks mentioned above, target analysis (NMR and EPR polarimetries and density, J. Singh, V.

Sulkosky and P. Solvignon, Temple U.), raster analysis (V. Sulkosky) and scintillator analysis (J. Singh). Longer term plan includes a final elastic analysis (J. Singh and USTC group) for both first and second periods. Cross sections and asymmetries (V, Sulkosky, J. Singh, J. Yuan) and radiative corrections (T. Averett, Col. of William and Mary) will be extracted for the second period. The same quantities will be extracted for the first period (J. Singh and USTC group) once the second period analysis is complete.

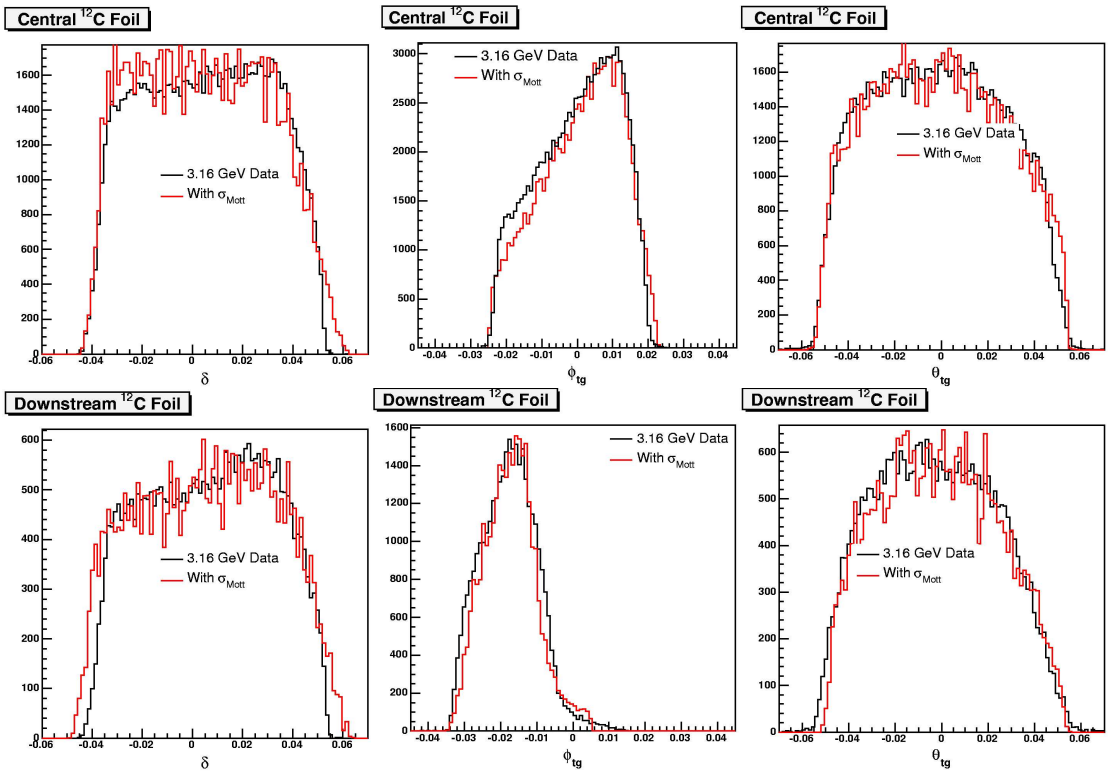

Figure 17: *Target reconstructed variables for the central (top plots) and downstream (bottom plots) carbon foils. The left plots are for dp/p, the middle plots are for the horizontal angle ϕ and the right ones are for the vertical angle θ. The data, taken at HRS momentum E'=3.16 GeV and 6^o angle, are shown with the black line. The red is for the SNAKE simulation results weighted by the Mott cross section.*

3.3 E99-115 and E00-114

A Study of the Strange Content of the Nucleon via Parity Violating Asymmetries in the $\vec{e}\,p \to e\,p$ and $\vec{e}\,^4He \to e\,^4He$ reactions.

D. Armstrong, G. Cates, K. Kumar, D. Lhuillier and R. Michaels, Spokespersons,
and
the Hall A Collaboration.

The HAPPEx-II experiments measure the parity violating asymmetry in elastic scattering of polarized electrons from ^1H and ^4He. This asymmetry is proportional to the Z^0 exchange which is used as a new probe of the nucleon structure. By analogy to the electromagnetic form factors $G_E^{\gamma p}$ and $G_M^{\gamma p}$ the nucleon weak vertex is parametrized by the weak form factors G_E^{Zp} and G_M^{Zp}. Assuming charge symmetry between the proton and neutron one can combine these two sets of form factors with the electromagnetic form factors of the neutron and extract the contribution of the three lightest quark flavors to the vector matrix element of the nucleon. Since the contribution of the strange quarks (G_E^s and G_M^s) comes only from the $s\bar{s}$ fluctuations of the quark sea a clean measurement of these observables provides new insight of the role of the fundamental degrees of freedom of QCD and their dynamics in the non-perturbative structure of the nucleon.

At tree level the parity violating asymmetry from protons is given by

$$\begin{aligned} A^{\rm PV} &= -\frac{G_F|Q|^2}{4\pi\alpha\sqrt{2}} \times \Bigg[(1-4\sin^2\theta_W) \\ &\quad -\frac{\epsilon G_E^{\gamma p}(G_E^{\gamma n}+G_E^s)+\tau G_M^{\gamma p}(G_M^{\gamma n}+G_M^s)-(1-4\sin^2\theta_W)\epsilon' G_M^{\gamma p} G_A^e}{\epsilon\left(G_E^{\gamma p}\right)^2+\tau\left(G_M^{\gamma p}\right)^2}\Bigg] \end{aligned} \tag{2}$$

where G_A^e is the axial form factor of the nucleon coming from the vector-axial structure of the weak neutral current. This term contributes significantly to $A^{\rm PV}$ only at backward scattering angle (θ) due to the kinematic factors ϵ, τ and ϵ', functions of θ and the beam energy (E). The HAPPEx measurements take place at very forward angles where the main contributions are electric and magnetic. A first experiment occurred in 1998-99 and measured [**?**] the combination $G_E^s + 0.392 G_M^s = 0.014 \pm 0.020 \pm 0.010$, compatible with zero at $Q^2 = 0.47\,GeV/c^2$. This result has demonstrated the high "parity quality" of the CEBAF beam and prompted a second generation of HAPPEx experiments. The strategy is to seek a possibly larger contribution at a lower Q^2 ($0.1\ GeV/c^2$) and to separate the electric and magnetic contributions by making measurements on the proton and an isoscalar target, only sensitive to G_E^s. The ^4He nucleus is chosen for its small and well controlled effect of the nuclear structure. The tree level asymmetry is given by

$$A^{\rm PV} = \frac{G_F|Q|^2}{4\pi\alpha\sqrt{2}}\left(4\sin^2\theta_W + \frac{2G_E^s}{G_E^{\gamma p}+G_E^{\gamma n}}\right) \tag{3}$$

A first run was conducted in summer 2004, collecting approximately 10% of the proposed statistics on the helium target and approximately 30% with the hydrogen target. As discussed below, results from these initial measurements have been submitted

for publication. Each measurement was then concluded in a run period covering the second half of 2005.

The figure of merit for these measurements grows toward high E and small θ leading to optimal kinematics $E = 3\ GeV$ and $\theta = 6$ degrees. The proposed precision on asymmetries and constraints on the strange form factors at $Q^2 = 0.1\,\mathrm{GeV}^2$ are listed in Table 5. The control of the systematic error at the 40 ppb level for hydrogen as well as the normalization at the 2% level for helium were the main challenges taken up by these

	A^{PV}	δA_{stat}	δA_{syst}	Sensitivity
H	-1.60	0.08 (5%)	0.04 (2.5%)	$\delta(G_E^s + 0.08 G_M^s) = 0.010$
^4He	+7.8	0.18 (2.2%)	0.18 (2.2%)	$\delta G_E^s = 0.015$

Table 5: Asymmetries and precision for H and ^4He targets, as proposed. When not specified all asymmetries are quoted in ppm units.

experiments. They required a specialized instrumentation in Hall A and an improved control of the noise and asymmetries in the beam parameters.

Figure 18 illustrates the experimental setup. The polarized electron beam is directed onto a 20 cm long cryogenic target and electrons scattered at 6° are detected in the Hall A High Resolution Spectrometers (HRS) configured symmetrically to double the rate. Because the HRS are physically unable to approach closer than 12.5°, an additional superconducting dipole (septum magnet) is installed in front each spectrometer. The expected high statistical precision on tiny physics asymmetries requires to run at very high luminosity leading to huge elastic rates in each spectrometer, up to 65MHz for hydrogen. The experiments take advantage of the HRS magnetic optics which focuses the elastic events in the focal plane along a line 50 cm away from the pion threshold events, the first inelastic background. The detector is a dedicated total absorption Cerenkov calorimeter, composed of alternating layers of quartz and brass, positioned above the elastic line. A custom made ADC integrates the light flux, proportional to the total energy deposited, over each helicity gate (33 ms). The standard detection package of the HRS can't operate at high rate in production mode. It is used only during dedicated runs at very low current ($\approx 1\mu$A) for detailed background studies and measurement of the mean Q^2 intercepted by the detector. In production mode a cross-check and monitoring of the rate distribution across the focal plane is performed by a scanner sweeping the acceptance.

The combination of an intense beam and an extended target can induce density fluctuations inside the target cell which would add to the pure statistical width of the counting rate and potentially affect the accuracy of the measurement. To keep this effect small, data were taken with "race track" type target cells. With this new geometry the coolant flow is transverse to the beam axis, dissipating the heat load in a more efficient way. To monitor the target fluctuations, eight dedicated luminosity detectors are installed around the beam axis at very forward angle (0.5°), where the statistical width is a lot smaller than in the detectors. Surprisingly, density fluctuations occured in both the liquid H_2 and dense cryogenic gas ^{4}He target. In both cases, the noise induced by these fluctuations could be reduced by increasing the size of the rastered beam spot. A large rastered beam spot, approximately 7x3 mm, was used during the 2005 run

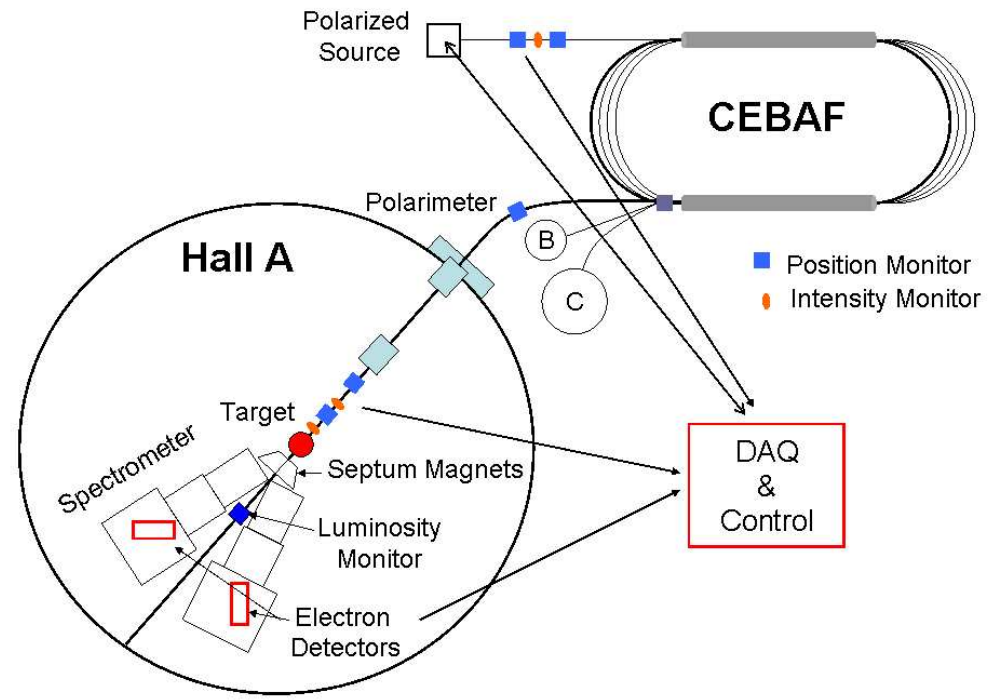

Figure 18: Overview of HAPPExII experiment.

period, and density fluctuations were suitably controlled for each measurement.

One major challenge for achieving high absolute precision is the control of helicity-correlated changes in the beam parameters which arise primarily from laser optics in the electron source. A feedback loop connecting the beam current readout in Hall A and the laser intensity modulation at the source was used to reduce the charge asymmetry of the electron beam. The HAPPEx collaboration, working closely with the CEBAF Electron Gun Group, has dedicated significant resources to identifying sources of position differences and reducing them by a careful setup of polarization and transport system for the laser beam. The positions at the target strongly depend on the beam optics and are more difficult to control via a feedback loop than the intensity. In addition to the careful setup at the source, the HAPPEX experiments rely on the "damping" of the position differences inherent in the acceleration of the electron beam as well as on the control of the beam tune at the target.

In the first portion of the 2005 run, control of position differences was compromised by beam motion caused through electrical pickup of the helicity generation signal. Only the measurement from the helium target, which is less demanding in terms of beam specifications, was affected by this problem. The problem was corrected before the more-demanding hydrogen target measurement. In addition, CASA physicists performed a careful matching procedure to reduce phase-space coupling of the beam before the hydrogen run. This procedure, which was under development for several years, was successful in improving the benefit of adiabatic damping of transverse beam motion. This improvement, combined with the careful configuration of the polarized source,

produced position differences which averaged to approximately 1 nm over the course of the hydrogen run. Example results for helicity-correlated beam motion during the 2005 hydrogen run are shown in Figure 19.

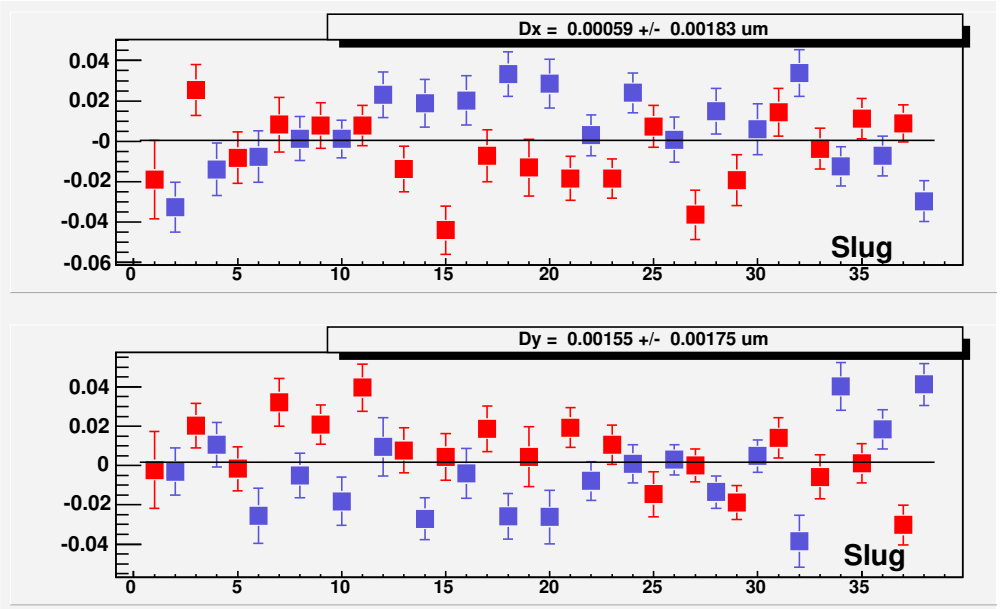

Figure 19: Example results for position differences, plotted per data "slug", during the 2005 run of HAPPEX-H. Units are micron, average results over the run are $\sim$ 1nm.

The beam polarization is continuously monitored by the Hall A Compton polarimeter with a few cross-check points from the Moller polarimeter in Hall A and the Mott polarimeter in the injector. Following the successful first use of the new "superlattice" photocathode technology at CEBAF during the 2004 Helium measurement, this type of photocathode was used to provide polarization in excess of 85% during the entire 2005 HAPPEX run.

The analysis of the 2004 data has been completed and results submitted for publication [?,?]. The $A^{\rm PV}$ and corresponding strange quark vector form factors were measured to be:

$$\begin{aligned} A^{PV}_{He}(Q^2 = 0.091\,\mathrm{GeV}^2) &= +6.72 \pm 0.84_{(stat)} \pm 0.21_{(syst)} \\ G^s_E(Q^2 = 0.091\,\mathrm{GeV}^2) &= -0.038 \pm 0.042_{(stat)} \pm 0.010_{(syst)} \end{aligned} \tag{4}$$

for the helium target and

$$\begin{aligned} A^{PV}_{H}(Q^2 = 0.099\,\mathrm{GeV}^2) &= -1.14 \pm 0.24_{(stat)} \pm 0.06_{(syst)} \\ G^s_E + 0.08 G^s_M(Q^2 = 0.099\,\mathrm{GeV}^2) &= 0.030 \pm 0.025_{(stat)} \pm 0.006_{(syst)} \pm 0.012_{(FF)} \end{aligned} \tag{5}$$

for the hydrogen target. The third uncertainty quoted for $G^s_E + 0.08 G^s_M$ accounts for uncertainty in the electromagnetic form factors (mainly $G^{\gamma n}_E$).

The two above combinations of strange form factors draw two bands in the $G^s_M - G^s_E$ plane, illustrated in Figure 20. Also shown are the results from the PVA4 experiment

at MAMI [?] and SAMPLE experiment at MIT-Bates [?] which measure complementary combinations at the same Q^2, and an estimated result extrapolated from three (lowest Q^2) data points from the G0 experiment at Jefferson Lab [?]. Taken together, these

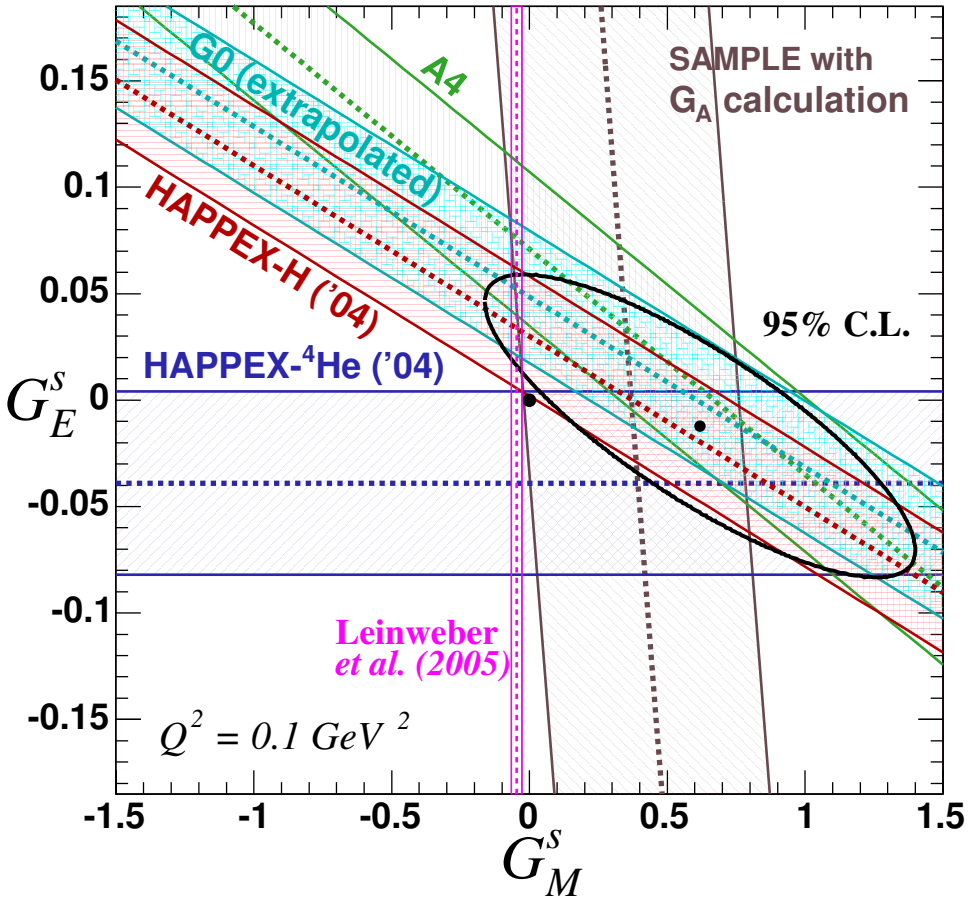

Figure 20: HAPPEx-H and HAPPEx-He results from 2004 run, with results from PVA4 [?] and SAMPLE [?] and extrapolated result from G0 [?]. The ellipse corresponds to the 95% confidence level contour.

measurements suggest a positive G_M^s although the deviation is not yet statistically conclusive.

The analysis of the 2005 data set is underway. Initial indications are that the systematic uncertainties will be controlled at or better than those for the 2004 data set. The final statistical uncertainty from 2005 is expected to be:

$$\begin{aligned} \delta(G_E^s) &= 0.014 \\ \delta(G_E^s + 0.084 G_M^s) &= 0.012 \end{aligned} \tag{6}$$

This precision should either establish a deviation from zero or constrain the strange content of the nucleon at low Q^2 to a negligible level.
HAPPEX04-H: nucl-ex/0506011.

HAPPEX04-He: Phys. Rev. Lett. **96** (2006) 022003.
G0: Phys. Rev. Lett. **95** (2005) 092001.

3.4 E00-007

Recoil Proton Polarization in Deuteron Photodisintegration at 2 GeV

X. Jiang with
R. Gilman, R. Holt, and Z.-E. Meziani, Spokespersons,
and
the Hall A Collaboration.

Deuteron photodisintegration provides high momentum transfers and high center of mass energies at modest photon energies. Thus, it has been a preferred reaction for developing a practical understanding of the transition between low energy hadronic degrees of freedom and high-energy quark and gluon degrees of freedom. Above one GeV photon energy at $\theta_{\rm c.m.} = 90^\circ$, cross sections largely follow the quark scaling rules, and are in general consistent with several quark-based theoretical approaches – note that some of these predict only the scaling behavior and not the absolute magnitude of the cross sections. Hadronic calculations are in general unsatisfactory, both on theoretical grounds and in the agreement between data and theory. See [14] for further details.

In Hall A experiment E89-019 [15], we showed that the high energy recoil proton polarizations at $\theta_{\rm c.m.} = 90^\circ$ smoothly vary with energy, with the induced polarization consistent with vanishing. These behaviors are what one would expect from a quark model, but not from a hadronic model in which resonance-background interferences tend to generate structures in the polarizations. Experiment 00-007 was developed to further test this behavior, with the measurement of an angular distribution of the recoil polarizations at 2 GeV photon energy, the highest energy at which such an experiment can be run in a reasonable time.

The experiment ran during the Fall of 2002. We made use of the FPP configured with a dual analyzer. The front FPP chambers were positioned between the extra CH_2 analyzer and the standard carbon analyzer, to improve efficiency, for four of our five kinematic points. The experiment also used the G0 helicity pulse structure, the first use of this pattern in Hall A. It employs quads of pulses, configured as $+--+$ or $-++-$, to more optimally remove potential small false asymmetries of concern to parity experiments. Data were taken at five angles.

The analysis has progressed over the years with the gradual resolution of several potentially serious technical problems, including inconsistencies / readout problems of the helicity information, and backgrounds related to the target being oriented skew to the beamline, particularly in our most forward angle setting.

The analysis work is now approaching completion, with preliminary results reported at DNP2005. A draft publication is expected by early 2006. The polarization transfer results are stable, insensitive to various cuts or variations in the analysis procedure. Calibration data taken with elastic *ep* scattering show consistent results for the carbon and CH_2 analyzers. The extracted values of the proton form factor ratio $\mu G_E/G_M$ are consistent with previous recoil polarimetry results – the ratio decreases with momentum transfer – but with less statistical precision due to these being short calibration runs.

Preliminary values for the photodisintegration polarization transfers are shown in Fig. 21. The two analyzers give consistent results, although the uncertainties are large at $\theta_{\rm c.m.} = 90^\circ$ for $C_{z'}$, due to the spin transport. The data are also in reasonable

agreement with the previous results from [15], which were taken at a beam energy about 100 MeV lower. We see that the quark gluon string (QGS) model [16] gives a good qualitative prediction for the longitudinal polarization transfer $C_{z'}$, in that it is large at forward angles and tends to decrease with angle. The hard rescattering model (HRM) [17] predicts that $C_{x'}$ is small, positive, and decreasing with angle, while the data instead are small, negative, and increasing with angle. Because $C_{x'}$ is sensitive to phases of amplitudes, while $C_{z'}$ is not, $C_{x'}$ is likely harder to predict precisely.

The induced polarization in ep elastic scattering results entirely from two-photon exchange, and is small, or order 0.01. Thus we have used the ep elastic scattering to calibrate the false asymmetry of the polarimeter, so that the induced polarization can be extracted for $\gamma d \to pn$. We do not report the p_y results at this point pending consistency checks between the two analyzers and final studies of sensitivity to variations in cuts. False asymmetries due to the FPP straw chamber inefficiencies and geometrical variations present a significant challenge to the p_y analysis, particularly the systematic uncertainties. The false uncertainties, however, are not be expected to affect the polarization transfer results.

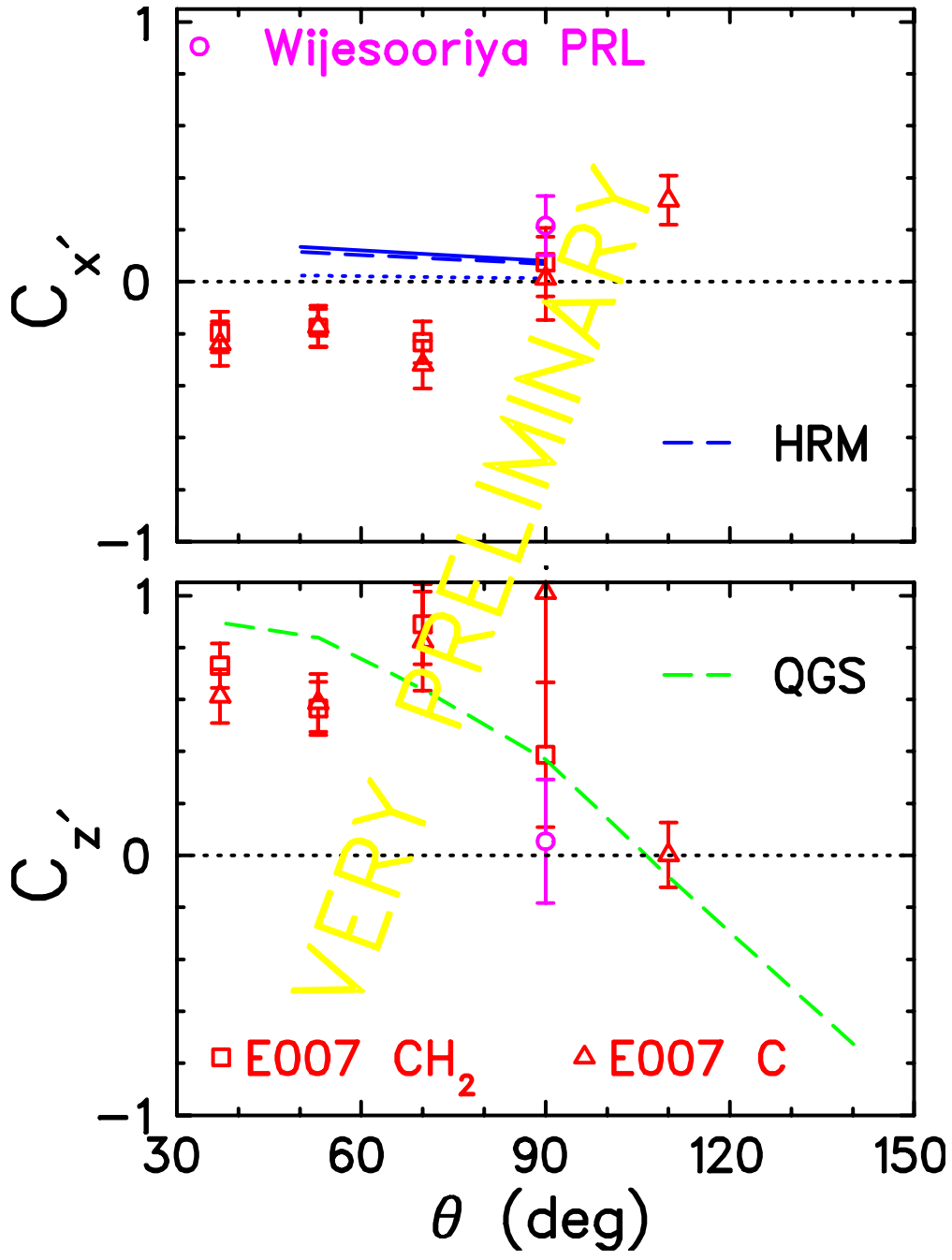

Figure 21: *The polarization transfer coefficients for $\gamma d \rightarrow pn$.*

3.5 E00-102

Testing the Limits of the Single-Particle Model in ^{16}O(e,e′p)

A. Saha, W. Bertozzi, L.B. Weinstein, and K. Fissum, spokespersons.

Experiment E00-102 is an update to Hall A experiment E89-003: Measurement of the cross section, R_{LT}, and A_{LT} for the ^{16}O(e,e′p) reaction. Experiment E89-003 made measurements at energy and momentum transfer of $\omega = 0.445$ GeV and $Q^2 = 0.8$ GeV^2 respectively, up to $p_M = 0.345$ GeV/c [34,35,36]. This update experiment expands these measurements up to $p_m = 0.755$ GeV/c at $\omega = 0.449$ GeV and $Q^2 = 0.902$ GeV^2. The goals of these measurements are to determine:

- the limits of validity of the single-particle model of valence proton knockout;
- the effects of relativity and spinor distortion on valence proton knockout using the diffractive character of the A_{LT} asymmetry; and
- the bound-state wave function and spectroscopic factors for valence knockout.

The cross section will be determined for measurements from p_m = -0.515 GeV/c to p_m = 0.755 GeV/c, in order to determined the point at which single-knockout calculations fail and two-nucleon effects become important. R_{LT} and A_{LT} will be separated for p_m up to ±0.515 GeV/c to further test the relativistic DWIA calculations. Fig 22 shows anticipated data points from E00-102 for A_{LT} as a function of missing momentum for the 1p-shell states along with data obtained from E89-003, both compared to calculations from Udias *et al.*

Data were taken at a fixed beam energy of 4.620 GeV, $\vec{q}$ = 1.066 GeV/c, and θ_q = 56.22°. Throughout the entire experiment, the electron arm (HRS-L) was fixed at 12.5° with a central momentum of 4.121 GeV/c, allowing it to be used as a luminosity monitor. The hadron arm (HRS-R) angle was varied from 28.3° to 96.1° to cover the necessary missing momentum range. These kinematics are shown in Fig 23.

Both detector stacks were used in their standard configurations. Each stack contained an additional S0 scintillator for checking trigger efficiency, and the HRS-L contained a pion rejector to be used for e^-/π^- separation. The target used was the Hall-A self-normalizing three-foil waterfall target [37, 38]. Each water foil was approximately 200 mg/cm^2 thick and separated by 25.4 mm. The foils were rotated to an angle of 57.4° with respect to the beam direction. Using the hydrogen in the water precise calibrations can be made as well as normalization of cross sections to known ^{1}H(e,e′p) and ^{1}H(e,e′) cross sections.

Detector calibrations, beam position and beam energy calibrations have been performed. Optimized detector maps have been created, and the data have been replayed using ESPACE. Analysis of the spectrometer mispointing has been performed. The water foil thicknesses have been determined by comparison of ^{16}O(e,e′p) yields to a BeO target of known thickness, and preliminary comparison of measured ^{1}H(e,e′p) yields to simulation have been made. An analysis of the electronic deadtime measurement is in progress. After that, oxygen cross sections, along with R_{LT} and A_{LT} will be extracted.

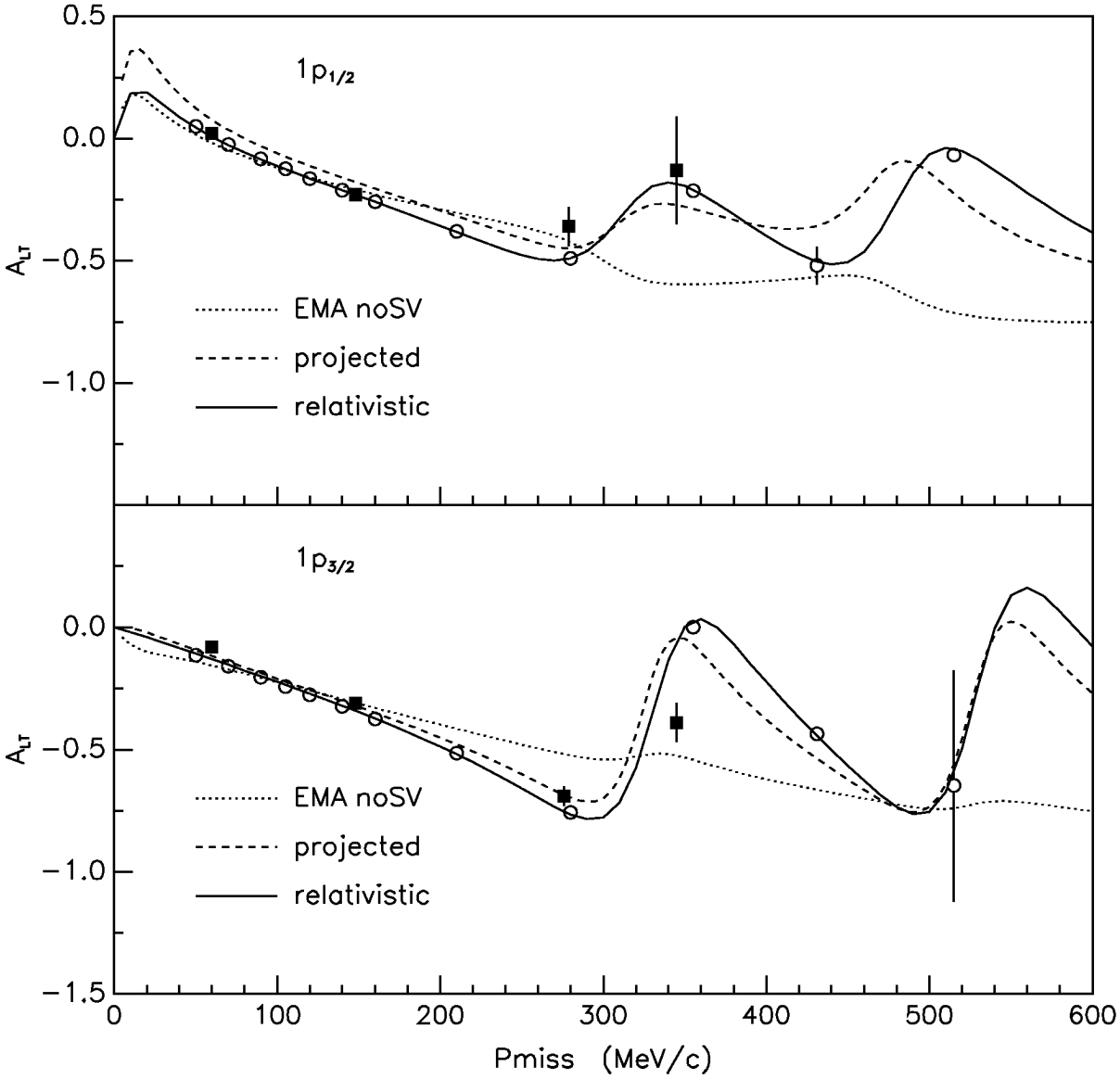

Figure 22: Projected A_{LT} data compared to E89-003 results and calculations of Udias *et al.* Open circles are anticipated data points from E00-102, solid squares are E89-003

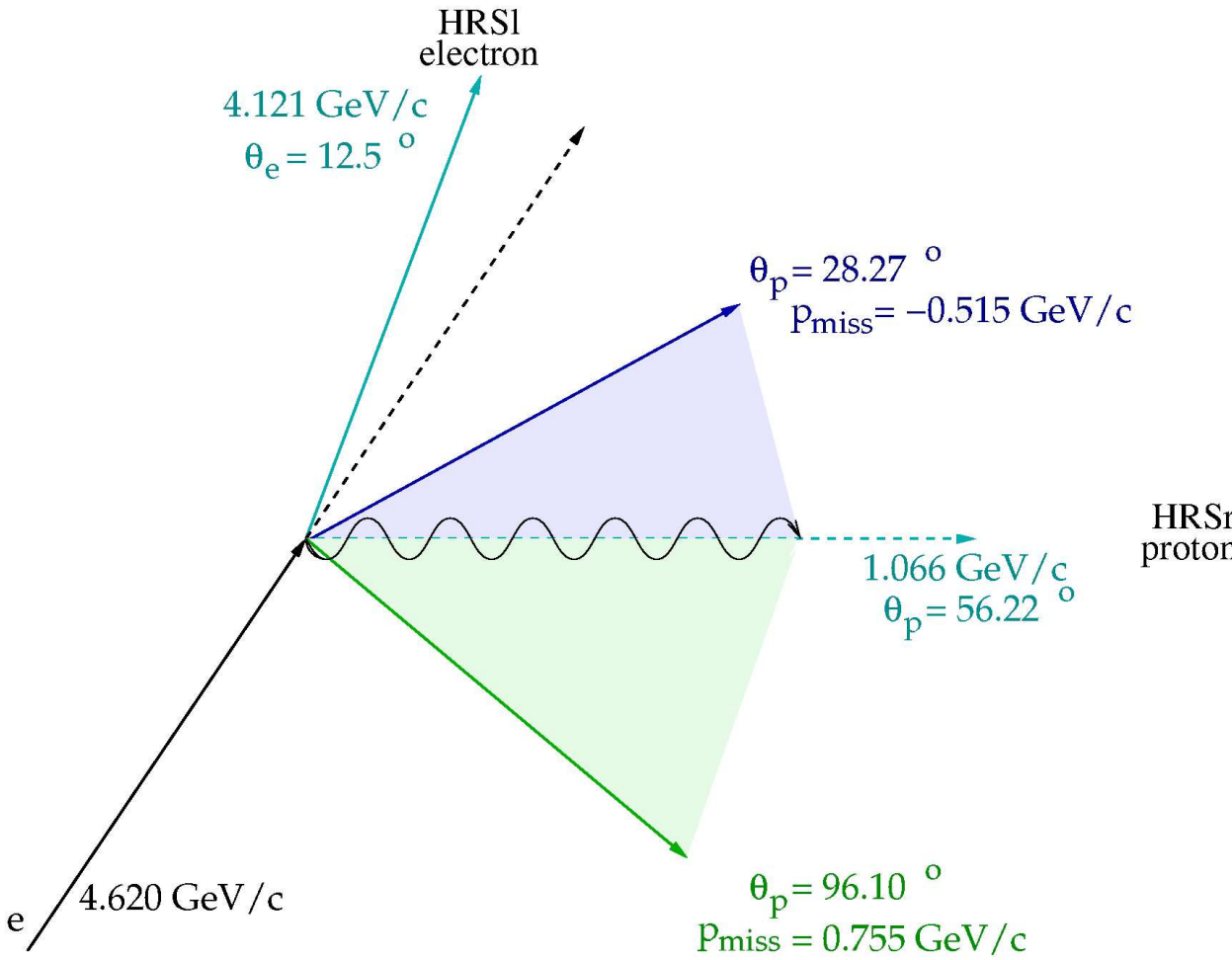

Figure 23: E00-102 kinematics. The beam energy was fixed at 4.620 GeV, and the HRS-L remained fixed at 12.5° with a central momentum of 4.121 GeV/c. The HRS-R was varied around the direction of parallel kinematics to cover the necessary missing momentum range.

3.6 E00-110 and E03-106

Deeply Virtual Compton Scattering on the proton and neutron

P. Bertin, C. Hyde-Wright, R. Ransome, F. Sabatié and E. Voutier
for the DVCS/Hall A Collaboration.

Deeply Virtual Comton Scattering (DVCS) aims to study the structure of the nucleon through the reaction $eN \to eN\gamma$ at high Q^2, high s and low t. A QCD factorization theorem states that in the Bjorken regime, the DVCS amplitude factorizes into the convolution of a hard kernel -calculable using perturbation theory- and a set of ground-state matrix elements, also known as the Generalized Parton Distributions (GPD). The GPDs are functions of x, $\xi \approx x_B/(2-x_B)$ and t, where $x \pm \xi$ are the lightcone momentum fractions of the active quark in the initial and final states. t can be interpreted as the Fourier conjugate to the transverse coordinate of the struck quark relative to the center-of-momentum coordinate.

Both DVCS experiments aimed at measuring the photo electroproduction cross-section difference for electrons of opposite helicities as a function of the variables Q^2 and t at fixed x_B=0.35. This observable is dominated by the interference between the Bethe-Heitler amplitude (radiation from the incident or scattered electron) and the DVCS amplitude constrained to the locus $x = \pm\xi$:

$$d^5 \overrightarrow{\sigma} - d^5 \overleftarrow{\sigma} \propto A \sin\varphi + B \sin 2\varphi \,. \tag{7}$$

The variable φ is the azimuthal angle between the leptonic and hadronic planes. The $A \sin\varphi$ term is the leading-twist contribution to this cross-section difference, and can be expressed as a linear combination of three twist-2 GPDs $\mathcal{H}$, $\tilde{\mathcal{H}}$ and $\mathcal{E}$:

$$A = F_1\mathcal{H} + \frac{x_B}{2-x_B}(F_1+F_2)\tilde{\mathcal{H}} - \frac{t}{4M^2}F_2\mathcal{E}\,, \tag{8}$$

where F_1 and F_2 are the usual elastic form factors.

In these DVCS experiments, the scattered electron is detected using the left HRS, the photon is detected in a compact 132-element PbF_2 calorimeter and the recoil nucleon was detected in the so-called Proton Array (PA), a 100-block plastic scintillator array.

In the neutron experiment, an additional veto detector was placed before the proton array to be able to discriminate between protons and neutrons entering the recoil detector. The charged particle tagger consists of 57 scintillating paddles distributed in two overlapping layers and placed in front of the PA. A charged particle going through this assembly is supposed to fire the PA and one PMT in each tagger layer while a neutral particle should not give any signal in the tagger. This logic is the basis of the DVCS analysis on the deuterium target and helps not only to tag charged particles but also to improve the selection of the exclusive channel. The performances of the tagger&PA association are illustrated on Fig. 24 where the energy deposit in each detector is reported after calibration of the energy conversion coefficients with protons associated to pion production. On the left panel, a clear band of events is identified corresponding

to protons: above 700 MeV/c, particles dont stop in the PA and their energy deposit decreases. The right panel is the first attempt for a ΔE/E identification of protons: it shows, in agreement with expectations, that a significant amount of protons stop in the tagger.

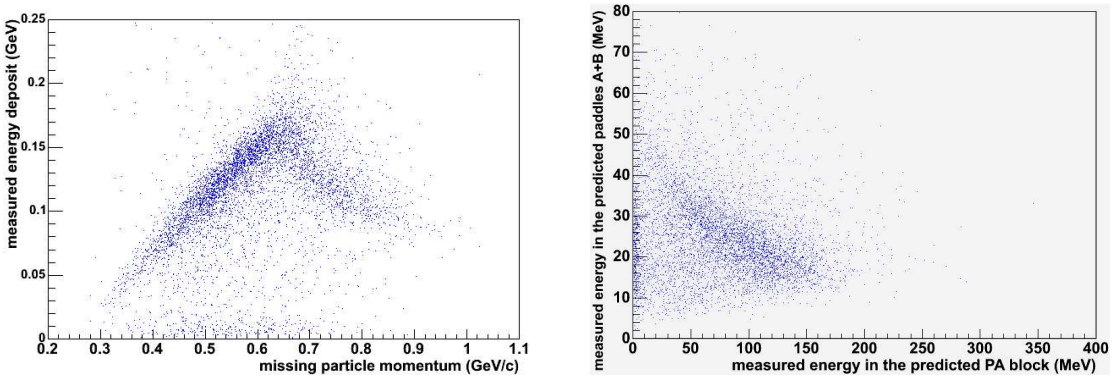

Figure 24: Left: measured energy deposit in the PA versus the reconstructed missing particle momentum. Right: measured energy deposit in the tagger assembly versus the measured energy deposit in the PA.

Each electronic channel of the custom detectors was digitized using 1 GHz analog ring samplers (ARS). This implied that the quantity of recorded data was rather high for a Hall A experiment, around 4 TBytes. A customized version of the C++ Hall A Analyser using a waveform analysis algorithm was used to reduce the amount of raw data and treat pile-up events. Most of the data processing was performed during the first half of 2005, the physics analysis itself began in the fall.

The first goal of the proton experiment E00-110 was to check whether or not the handbag approximation was valid at moderate $Q^2 \sim 2$ GeV^2. For this purpose, a scan in Q^2 from 1.5 to 2.5 GeV^2 was performed at fixed x_B=0.35. For each setting in Q^2 and t, we performed a model-independent extraction of the different terms entering both the difference and sum of helicity-dependent cross-sections. From this analysis, we found out that Q^2 as low as 2 GeV^2 ware sufficient in order to be in the handbag-dominance regime. This allows for the extraction of linear combination of GPDs entering in the BH-DVCS interference term, which is still under way.

For the neutron experiment E03-106, the extraction of cross-section differences and relative asymmetries is pursued according to two complementary methods: exclusive and semi-exclusive. The former uses the complete detector assembly to select the DVCS reaction on a quasi-free neutron in order to sign the possible existence of a DVCS asymmetry in the neutron channel. The latter, which involves the HRS and the DVCS calorimeter only, will be used to study the t-dependence of the reaction.

Overall, data analysis is well underway and very interesting results on both proton and neutron targets will be shown in conferences starting in 2006.

3.7 E01-012

Measurement of neutron (^{3}He) spin structure functions in the resonance region.

J. P. Chen, S. Choi, N. Liyanage, spokespersons
P. Solvignon, graduate student

Experiment E01-012 ran in January and February, 2003. The goal of this experiment is to perform a precision extraction of the neutron spin structure function g_1^n and the virtual photon asymmetry A_1^n in the resonance region over a moderate Q^2 range (up to $Q^2 = 4(\mathrm{GeV/c})^2$) using Hall A polarized ^{3}He target. The results from this experiment, combined with Deep-Inelastic-Scattering data, will provide a precision test of quark-hadron (Bloom-Gilman) duality predictions for neutron spin structure function g_1^n and the virtual photon asymmetry A_1^n. The Bloom-Gilman duality has been experimentally demonstrated for spin independent structure function F_2. Duality is observed when the smooth scaling curve at high momentum transfer is an average over the resonance bumps at lower momentum transfer, but at the same value of scaling variable x_{Bj}. Results from E01-012 will enable one of the first precision tests of spin and flavor dependence of quark-hadron duality. The demonstration of duality for spin structure functions will enable the use of resonance data to study the nucleon spin structure in the very high x_{Bj} region.

In this experiment we used the polarized beam and the polarized ^{3}He target to measure the inclusive $^3\vec{H}e(e,e')X$ reaction. Both Hall A High Resolution spectrometers (HRS) were used in a symmetric configuration in electron detection mode. Three beam energies, 3 GeV, 4 GeV and 5 GeV were used with spectrometer angles of 25° and 32°. At each kinematic setting parallel and perpendicular asymmetries were measured with the target spin parallel and perpendicular to the electron beam respectively. The Q^2/W phase-space covered by this experiment is given in Figure 25.

Current Status: The analysis of E01-012 data is almost complete now. Figure 1 (left) shows preliminary results for $A_1^{^3He}$ in the resonance region at the four Q^2 values, compared to $A_1^{^3He}$ in the DIS region from Hall A experiment E99-117 [43]. The position of the $\Delta(1232)$ resonance is indicated by an arrow. The error bars shown are statistical only. The most noticeable feature of the plot is the negative contribution due to $\Delta(1232)$ at the two low Q^2 settings ($Q^2 < 2\ (GeV/c)^2$). It has been noted that quark-hadron duality for spin structure functions is not expected in the Delta resonance region at this low Q^2. For the two higher Q^2 settings, $A_1^{^3He}$ at the location of $\Delta(1232)$ is positive. It is also interesting to note that the results from these two settings ($Q^2 > 2\ (GeV/c)^2$) agree perfectly with each other, showing little or no Q^2 dependence, as expected in the scaling region. Furthermore, Our data seem to indicate that with increasing x_{Bj}, A_1 goes from negative to positive showing the same trend as indicated by the DIS data from Experiment 99-117. The behavior of A_1^n becoming positive at high x_{Bj} has been predicted for DIS data by relativistic constituent quark models and by pQCD inspired models [44].

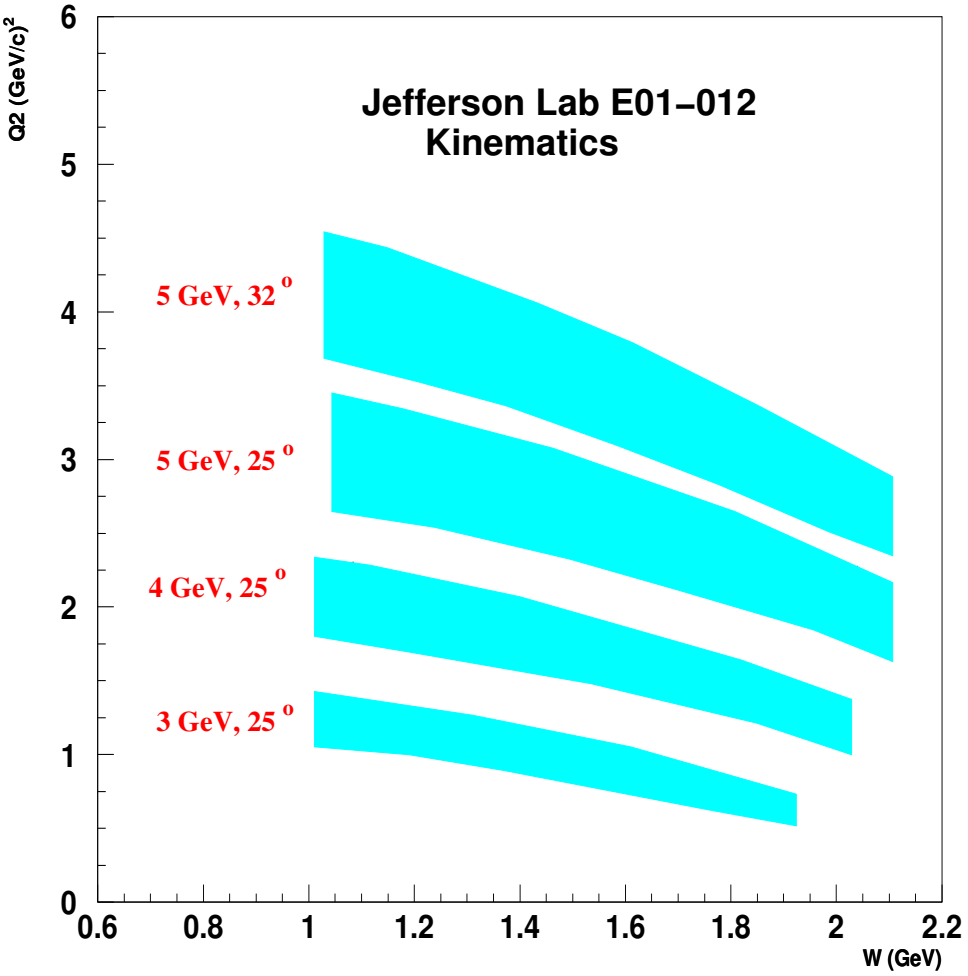

Figure 25: The Q^2 and W coverage for E01-012

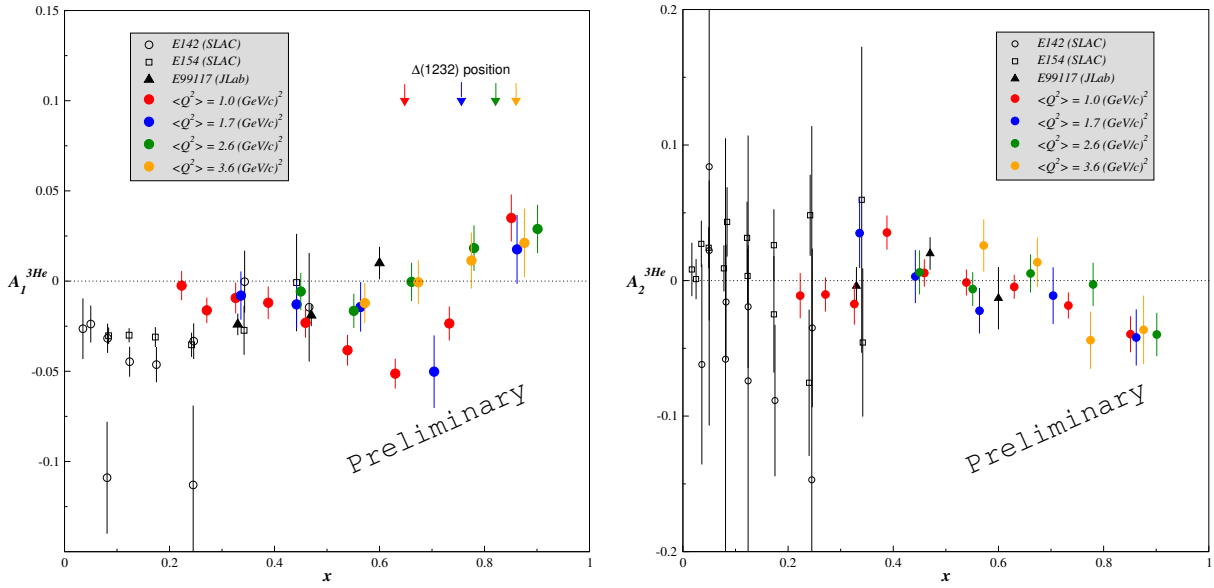

Figure 26: Preliminary results from Hall A experiment E01-012 for $A_1^{^3He}$ (left) and $A_2^{^3He}$ (right), compared $A_1^{^3He}$ and $A_2^{^3He}$ measured in the DIS region from Hall A experiment E99-117. The arrow indicates the location of the $\Delta(1232)$ resonance.

3.8 E01-015

Studying the Internal Small-Distance Structure of Nuclei via the Triple Coincidence (e,e'p+N) Measurement

D.W. Higinbotham
for the Hall A Collaboration.

Experiment E01-015 completed data taking in April of 2005 and analysis is now well underway. The experiment took ^{12}C(e,e′p) data with the two Hall A high resolution spectrometers while reading out the BigBite spectrometer (see Section 2.4) and a neutron detector for each left spectrometer trigger. There four Ph.D. students working on the analysis of the data. Peter Monaghan (MIT) is analyzing the ^{12}C(e,e′p) reaction, Ran Shneor (Tel Aviv University) is analyzing the $^{12}C(e,e'pp)$ reaction, Ramesh Raj Subedi (Kent State University) is analyzing the $^{12}C(e,e'pn)$ reaction, and Neil Thomson (University of Glasgow) is analyzing triple coincidence events where a deuteron was detected in either an HRS and/or in BigBite.

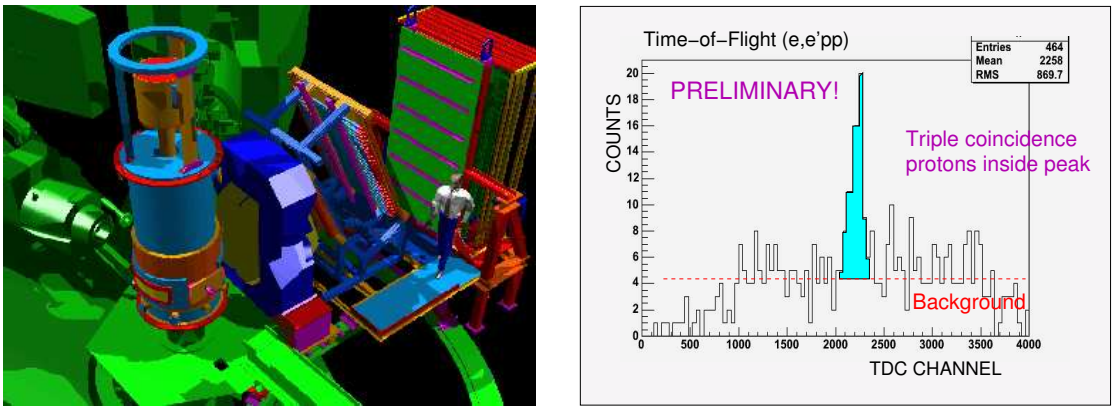

Figure 27: The left image shows a computer-aided design (CAD) drawing of the SRC experimental setup. The right image shows a preliminary timing peak from the $^{12}C(e,e'pp)$ reaction as detected by the two HRS and BigBite.

The left panel of Fig. 27 shows a computer-aided design (CAD) drawing of the short-range correlations (SRC) experimental setup. The BigBite spectrometer and the Hall A Neutron Detector (HAND) can be seen on the right side of the drawing. A preliminary analysis of triple coincidence $^{12}C(e,e'pp)$ events can be seen in the right side of the figure. The recoiling protons for this plot had momentum in excess of 500 MeV/c. For this experiment's $x_B > 1$ and high four-momentum transfer kinematics, such high momentum recoil events are likely due to correlations, though this will need to be confirmed by theoretical calculation. It is certainly a recoil momentum that is significantly higher than the Fermi momentum and the data is in a kinematics where final state interactions and meson exchange currents should be suppressed.

Fig. 28 shows triple coincidence events between the two HRS and HAND. The left panel shows the over-determined $D(e,e'pn)$ reaction which will be used to calibrate

HAND's absolute neutron detection efficency . The right panel shows the $^{12}C(e,e'pn$ data for recoil momentum of around 500 MeV/c. The SRC experiment was the first experiment in Hall A to use a neutron detector. In Hall A, we were able to operated the detector without a shield hut, only a lead wall was added between the target and the face of the detector's veto paddles to remove low energy background.

Figure 28: Shown on the left is the coincidence time spectrum from the over-determined $D(e,e'pn)$ reaction. Shown on the right is the coincidence time spectrometer for the $^{12}C(e,e'pn)$ reaction.

In summary, preliminary analysis has shown triple coincidence timing spectrums from both the BigBite spectrometer and the Hall A Neutron Detector (HAND). There several students working hard on the analysis of the SRC data so by next years annual report we should be able to present the ratios of the various reaction channels along preliminary cross section results.

3.9 E04-012

High-Resolution Search for $\Theta^+(1540)$ Partners

P. E. Reimer and B. Wojtsekhowski, Spokespersons,
and
the Hall A Collaboration.

Contributed by J.-O. Hansen

3.9.1 Introduction

Recent claims of the observation [47] of a narrow exotic $S = +1$ baryonic state, the $\Theta^+(1540)$, have generated considerable experimental and theoretical interest. If confirmed, the Θ^+ could be the lowest-mass member of an antidecuplet of pentaquarks, which has been predicted in the framework of the Chiral Quark Soliton Model [48]. Other identifications are also possible. For example, the narrow width of the Θ^+ has been explained in terms of isospin-violating strong decays, which has led to the suggestion of an isotensor multiplet of pentaquarks [49].

If the Θ^+ pentaquark exists then other members of its symmetry group should be observable as well, provided that they are sufficiently narrow. Both the Chiral Quark Soliton Model and the isotensor multiplet model predict relatively narrow ($\Gamma < 30 - 50$ MeV) partner states in the mass region $M \approx 1500 - 2000$ MeV.

In the following, we report the results of a search for the possible Σ_5^0 and N_5^0 members of the antidecuplet and for the isotensor partner Θ^{++} which was carried out in Hall A last year. The reactions $ep \to e'K^+X$, $ep \to e'\pi^+X$ and $ep \to e'K^-X$ were investigated for evidence of narrow structures in the reconstructed missing mass (M_X). The measurements covered a limited range of forward scattering angles, which did not allow a partial-wave analysis. However, excellent mass resolution was achieved. Precise, high-statistics data of the known $\Lambda(1116)$, $\Sigma(1193)$ and $\Lambda(1520)$ resonances were obtained for calibration purposes. The results presented here are near final.

3.9.2 Experiment

The experiment ran in Hall A at Jefferson Lab in May 2004 using a 5 GeV continuous-wave electron beam incident on a 15 cm long liquid hydrogen target. Scattered electrons were detected in one of the Hall A High-Resolution Spectrometers (HRS) in coincidence with electroproduced hadrons that were measured in the second HRS. The experimental setup is illustrated in Figure 29. Both HRS were positioned at 6° forward angles, using septa on each arm to reach this small scattering angle. Each spectrometer had an effective acceptance of approximately 4 msr in solid angle and ±4.5% in momentum. For the production runs, to achieve the desired missing mass coverage, the central momentum of the electron HRS was stepped from 1.70 and 2.02 GeV/c, while the central momentum of the hadron HRS was changed between 1.89 and 2.10 GeV/c.

Both spectrometers used a QQDQ magnet arrangement for focusing and a 45° upward bend. The detector packages, placed behind the magnetic elements, were equipped with four planes of vertical drift chambers for tracking and two planes of fast hodoscopes

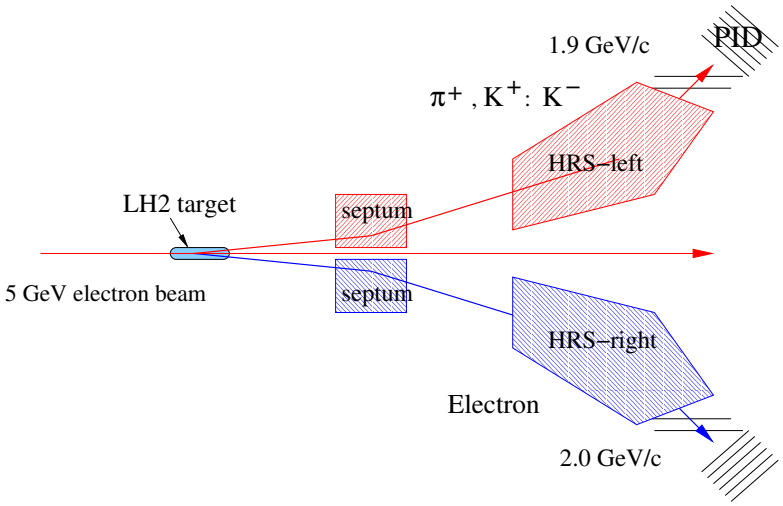

Figure 29: Experimental setup.

for triggering. Careful calibration of the trigger system yielded a coincidence timing resolution of 600 ps FWHM. The scattering vertex resolution of each spectrometer was 2.5 cm FWHM. The electron HRS employed a CO_2 gas Cherenkov counter for pion rejection. For the kaon measurements, clean particle identification in the hadron HRS was particularly important because of the very high ratio of π/K rates. For this purpose, the hadron HRS was instrumented with two aerogel and a ring-imaging Cherenkov detector as well as a lead glass shower counter. Combined with the coincidence time-of-flight measurement, a total pion rejection factor of 3×10^4 was achieved.

The average momentum transfer carried by the virtual photon was $Q^2 \approx 0.1$ (GeV/c)^2. For the kaon (pion) kinematics, the average center-of-mass scattering angle was $\theta^{CM}_{\gamma^* K} \approx 6^\circ$ ($\theta^{CM}_{\gamma^* \pi} \approx 7^\circ$), and the angular acceptance was $\Delta\Omega^{CM}_K \approx 40$ msr ($\Delta\Omega^{CM}_\pi \approx 30$ msr).

3.9.3 Analysis

The yields measured in each spectrometer were corrected for detector and trigger efficiencies and dead-time. Cuts on the data from the PID detectors were applied to select appropriate particle types, and vertex and coincidence time cuts were used to reduce background from accidentals. The missing mass, M_X, was reconstructed using the measured momenta of the electron and kaon (pion). The resulting spectra were corrected for the missing mass acceptance, which varied strongly within the mass range covered by each kinematic setting because of the limited momentum acceptance of the spectrometers. All spectra were normalized by luminosity.

Calibration data were taken in the $ep \to e'\pi^+ X$ channel in the mass range of the neutron, and in the $ep \to e'K^+ X$ channel covering the range where the $\Lambda(1116)$ and $\Sigma(1193)$ could be seen. The missing mass resolution was determined to be 3.5 MeV FWHM. Using the well-known masses of the calibration states, the accuracy of our reconstructed missing mass was determined to be better than 3 MeV.

In the search regions, the missing mass data from several kinematics (up to 8) were

combined to arrive at the final spectra used for the peak search analysis (see below). The individual data sets overlapped to some extent, allowing a check of the corrections and normalizations. After finalizing the detector analysis, all transitions were found to be smooth, requiring no ad-hoc scaling factors. Background was not subtracted from any of the spectra.

To quantify any possible observations (or non-observations), we performed a systematic search for peaks in the final missing mass spectra of the three reaction channels. Within a 50 MeV wide window, we fitted a linear background to the data. Then a Breit-Wigner peak convoluted with a Gaussian of width $\sigma = 1.5$ MeV was added to this background at the center of the window, the fit was repeated, and the difference of the χ^2 of the two fits, $\Delta\chi^2_{exp}(M_X)$,was recorded. Here, the Gaussian simulated the experimental missing mass resolution, and widths of $\Gamma = 1, 3, 5$, and 8 MeV were assumed for the Breit-Wigner function. This procedure was repeated after shifting the window across the measured missing mass range in steps of 2 MeV. For the Θ^{++} search, χ^2 was replaced with the log-likelihood because of the low statistics of the data. A strong improvement of χ^2 (or log-likelihood, respectively) indicated a candidate for a signal. The statistical significance of the most prominent peak candidates was determined using the standard method of computing the Poisson probability for the background (estimated from sidebands) to fluctuate to the observed signal, expressed in terms of Gaussian sigma.

To obtain upper limits on the production cross section, we carried out a Monte Carlo simulation. In this way, the details of our peak search procedure, the peak shape, experimental resolution, corrections, background fluctuations, etc. were accounted for. The Monte Carlo simulated the presence of a peak, whose cross-section σ_{MC} was varied from 0 to 20 nb/sr. The purpose was to find the correspondence between the Monte Carlo peak strength and the probability to find a certain χ^2 improvement, $\Delta\chi^2(\sigma_{MC})$, due to such a peak when applying the search algorithm described above to the Monte Carlo spectra. We define the quantity $\Delta\chi^2_{90}(\sigma_{MC})$ such that a Monte Carlo peak of cross-section σ_{MC} results in a χ^2 improvement *greater* than $\Delta\chi^2_{90}$ with 90% probability. Thus, if a value $\Delta\chi^2 = \Delta\chi^2_{90}(\sigma_{MC})$ is actually observed in the experiment, then we know that we may have missed a real peak of cross section $\sigma \leq \sigma_{MC}$ with only 10% probability. Hence, we can take the Monte Carlo cross section σ_{MC} for which $\Delta\chi^2_{90}(\sigma_{MC}) = \Delta\chi^2_{exp}$ as the 90% CL upper limit on the production cross section. The resulting values for our searches are given in Table 6.

3.9.4 Results and Conclusions

Figure 30 depicts the missing mass spectra obtained for the three reaction channels along with a fit to the most significant candidate peak found in each scan. The parameters of these peaks are given in Table 6. These results were obtained with an assumed width of $\Gamma = 5$ MeV for the Breit-Wigner function; other assumed widths yield very similar results, except that σ_{max} generally increases with increasing peak width, as expected. The table also gives the cross-section ratio of the respective largest peak to the cross section of the $\Lambda(1520)$ as measured in our experiment in the K^+ channel. There are several known or suspected resonances in our mass region [50], in particular several 3 or 4-star Λ and Σ states in the $ep \to e'K^+X$ channel. Most of these states are either wide

Channel	Mass value of largest peak (MeV)	Significance	Yield ratio to $\Lambda(1520)$	Cross section limit σ_{max} (nb/sr)
$ep \to e'K^+X$ (Σ_5^0)	1720	2.3σ	3.7%	8–16
$ep \to e'\pi^+X$ (N_5^0)	1855	2.5σ	2.0%	4–9
$ep \to e'K^-X$ (Θ^{++})	1570	3σ	1.4%	3–6

Table 6: Parameters of the largest observed bumps in each reaction channel. The range given for σ_{max} corresponds to the range $\Gamma = 1 - 8$ MeV of assumed widths used in the peak search.

(> 50 MeV) or have only been seen in partial-wave analyses. Taken together, they likely add up to a relatively smooth background. Still, we do see several broad structures in this channel, possibly the $\Sigma(1670)$ and $\Sigma(1775)$.

In conclusion, we do not observe statistically significant narrow ($\Gamma < 10$ MeV) structures in any of our three reaction channels. Any signals seen are consistent with background. Our experiment had a relatively small angular coverage, moderate statistics, and was kinematically incomplete, thus our ability to rule out pentaquark partner states or other narrow resonances in our search regions is naturally somewhat restricted.

3.9.5 Acknowledgements

Special thanks are due to our graduate student Yi Qiang from MIT, whose skills in data analysis and graphics presentation have been invaluable.

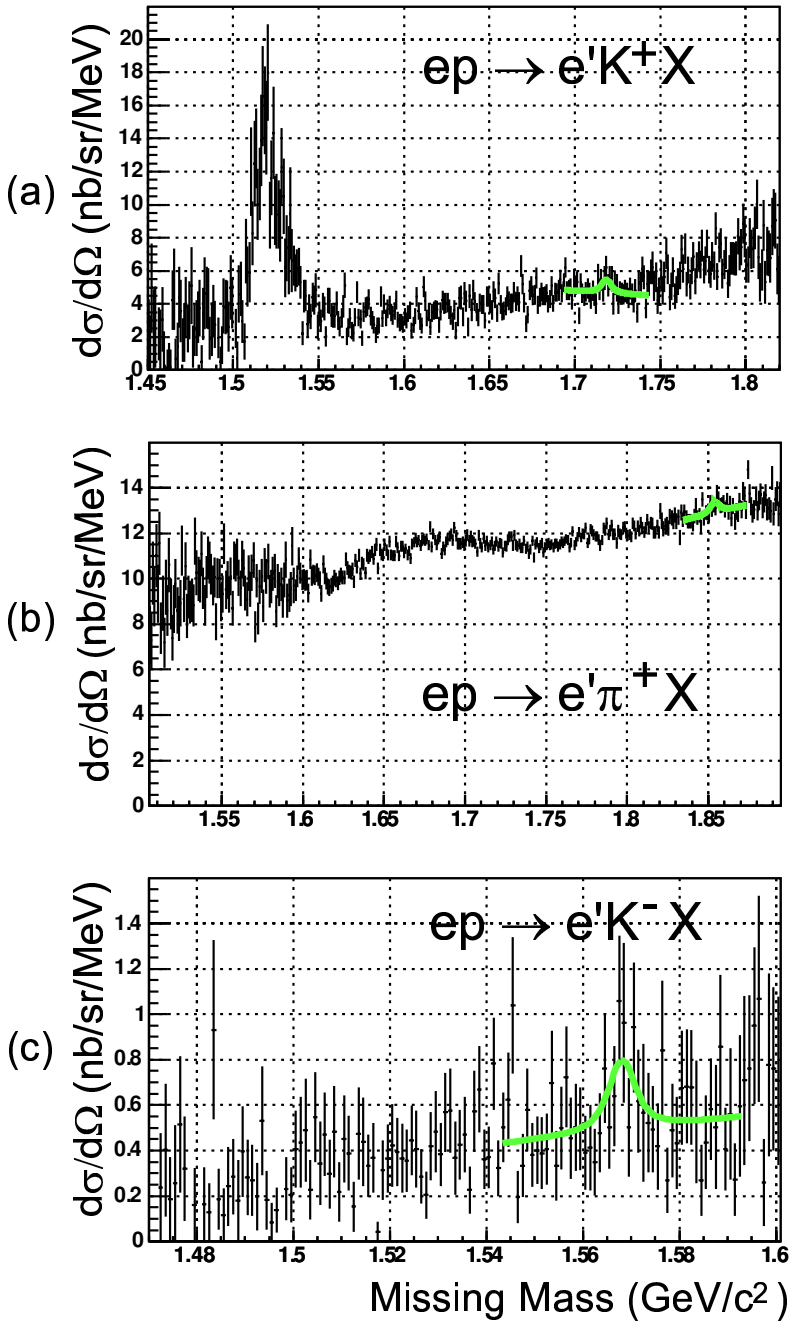

Figure 30: Final missing mass spectra obtained for the three reaction channels (a) $ep \to e'K^+X$ (Σ_5^0 search), (b) $ep \to e'\pi^+X$ (N_5^0 search), and (c) $ep \to e'K^-X$ (Θ^{++} search). The fits to the most significant peak are shown in each spectrum; the parameters of these peaks are listed in Table 6. A peak width of $\Gamma = 5$ MeV was assumed for the fits shown; other assumed widths yield similar results. The large peak in the K^+ channel (a) is the $\Lambda(1520)$.

References

[1] http:hallaweb.jlab.orgequipmenttargetscryotargets.

[2] W. Bertozzi, E. Piasetzky, J. Watson and S. Wood, spokespersons, JLab Experiment E01-015, *Studying the internal small-distance structure of Nuclei via the triple coincidence (e,e'p+N) measurement.*

[3] G. Cates, K. McCormick, B. Reitz and B. Wojtsekhowski, spokespersons, JLab Experiment E02-013, *Measurement of the neutron electric form factor G_n^E at high Q^2.* 11 15 15, 16

[4] W. Bertozzi, S. Gilad, D.W. Higinbotham, B.E. Norum and S. Širca, spokespersons, JLab Experiment E05-102, *Measurement of A_x and A_z asymmetries in the quasi-elastic polarized ^{3}He($\vec{e}$,e'd) reaction.* 15, 16

[5] J. Annand, D.W. Higinbotham, R. Lindgren and V. Nelyubin, spokespersons, JLab Experiment E01-014, *Precision measurement of electroproduction of π^0 near threshold: a test of chiral QCD dynamics.* 15, 16

[6] J.P. Chen, X. Jiang and J.C. Peng, spokespersons, JLab Experiment E03-004, *Measurement of single target-spin asymmetry in semi-inclusive pion electroproduction on a transversely polarized ^{3}He target.* 15, 16

[7] B. Wojsekhowski, P.E. Reimer and V. Nelyubin, spokespersons, JLab Experiment E05-013, *High Resolution Study of the Resonance in nK^+ System.* 15, 16

[8] J.-C. Peng, L.Y. Zhu, J.-P. Chen and X. Jiang, spokespersons, JLab Experiment E04-114, *A Measurement of the Flavor Asymmetry through Charged Meson Production in Semi-Inclusive Deep-Inelastic Scattering.* 15

[9] D. W. Higinbotham, *High Field BigBite Dipole Test*, TOSP PHY-05-015. 15

[10] D. W. Higinbotham, *High Field BigBite Dipole Procedure*, OSP PHY-05-001. 15

[11] Hall A 2004 Status Report

[12] J. Alcorn *et al.*, Nucl. Instrum. Meth. **A**522:294-346 (2004).

[13] http://alice-hmpid.web.cern.ch/alice 22 19, 22 23

[14] R. Gilman and F. Gross, J. Phys. G **28**, R37 (2002). 42

[15] K. Wijesooriya *et al.*, Phys. Rev. Lett. **86**, 2975 (2001). 42, 43

[16] V. Yu. Grishina *et al.*, Eur. Phys. J **A19**, 117 (2004). 43

[17] M.M. Sargsian, Phys. Lett. B **587** 41, (2004).

[18] `http://hallaweb.jlab.org/root/`

[19] Amy Orsborn, "Assessment of Hall A Vertical Drift Chamber Performance Through Monte Carlo Simulation", JLab TN-05-069

[20] S. Frullani, F. Garibaldi, J. LeRose, P. Markowitz, and T. Saito, High Resolution Hypernuclear 1p Shell Spectroscopy, Jefferson Lab experiment E94-107. 43 18 19

[21] M. Iodice *et al.*, *Nucl. Instrum. Methods* **A441**, 223 (1998).

[22] Corning 7980, Valley Design `http://www.valleydesign.com`. 25 25

[23] http://hallaweb.jlab.org/targets/polhe3/polhe3_tgt.html;
and tech notes in http://www.jlab.org/e94010/.

[24] M. Amarian *et al.*, Phys. Rev. Lett. 89, 242301 (2002); 92, 022301 (2004); 93, 152301 (2004); Z. Meziani,*et al.*, Phys. Lett. B 613, 148 (2005).

[25] W. Xu, *et al.*, Phys. Rev. Lett. 85, 2900 (2000); F. Xiong, *et al.*, Phys. Rev. Lett. 87, 242501 (2001).

[26] X. Zheng, *et al.*, Phys. Rev. Lett.92, 012004 (2004); Phys. Rev. C 70, 065207 (2004).

[27] K. Kramer, *et al.*, Phys. Rev. Lett. 95, 142002 (2005).

[28] JLab E01-012, Spokespersons, J. P. Chen, S. Choi, N. Liyanage.

[29] JLab E97-110, Spokespersons, J. P. Chen, A. Deur and F. Garibaldi.

[30] JLab E02-013, Spokespersons, G. Cates, K. McCormick, B. Reitz and B. Wojtsekhowski.

[31] E. Babcock, *et al.*, Phys. Rev. Lett. 91, 123003 (2003).

[32] JLab E03-004, Spokespersons, J. P.Chen, X. Jiang and J. C. Peng.

[33] JLab E05-015, Spokespersons, T. Averett, J. P. Chen and X. Jiang.

[34] W. Bertozzi, K.Fissum, A. Saha, and L. Weinstein, spokespersons, JLab Experiment E89-003, *Study of the Quasi-Elastic (e,e′p) Reaction in* ^{16}O *at High Recoil Momentum*. 21 21 21 21 21 21 21 21 21 21 21 45

[35] J.Gao *et al.*, Phys. Rev. Lett. **84**, 3265 (2000). 45

[36] N. Liyanage *et al.*, Phys. Rev. Lett. **86**, 5670 (2001). 45

[37] F. Garibaldi *et al.*, Nucl. Instum. Methods. Phys. Res. A **314**, 1 (1992). 45

[38] E. Cisbani *et al.*, *A Waterfall Target System for Hall A at Jefferson Lab*, INFN/ISS **97/04 (1997).** 45

[39] E. D. Bloom and F. J. Gilman, Phys. Rev. Lett. 25, 1140 (1970); Phys. Rev. D 4, 2901 (1971).

[40] I. Niculescu *et al.***, Phys. Rev. Lett. 85, 1186 (2000); I. Niculescu** *et al.***, Phys. Rev. Lett. 85, 1182 (2000).**

[41] A. Airapetian *et al.***, Phys. Rev. Lett. 90, 092002 (2003).**

[42] **W. Melnitchouk, R. Ent and C. Keppel, Phys.Rept. 406, 127-301 (2005).**

[43] **X. Zheng** *et al.*, **Phys. Rev. C 70, 065207 (2004); X. Zheng** *et al.*, **Phys. Rev. Lett. 92, 012004 (2004).**

[44] **See the discussion in X. Zheng** *et al.*, **Phys. Rev. C 70 and references therein.**

[45] **Vipuli Dharmawardane, Ph.D Thesis, Old Dominion University (2004)**

[46] **Yelena Prok, Ph.D Thesis, University of Virginia (2004).**

[47] **see, for example, S. Stepanyan** *et al.* **[CLAS collaboration], Phys. Rev. Lett. 91, 252001 (2003).** **50** **50** **55**

[48] **D. Diakonov, V. Petrov, and M. Polyakov, Z. Phys. A 359, 305 (1997).** **55**

[49] **S. Capstick** *et al.*, **Phys. Lett. B 570, 185 (2003).** **55**

[50] *Review of Particle Physics*, **S. Eidelman** *et al.*, **Phys. Lett. B 592, 1 (2004).**

57

4 Hall A Collaboration Member List

Armando Acha	*Florida International University*
Bryon Anderson	*Kent State University*
Mattias Andersson	*University of Lund*
Konrad A. Aniol	*California State University*
John Annand	*University of Glasgow*
David S. Armstrong	*College of William and Mary*
John Arrington	*Argonne National Laboratory*
Todd Averett	*College of William and Mary*
Maud Baylac	*Jefferson Laboratory*
Elizabeth Beise	*University of Maryland*
Hachemi Benaoum	*Syracuse University*
Fatiha Benmokhtar	*University of Maryland*
Jacques Berthot	*Université Blaise Pascal, Clermont-Ferrand*
Pierre Bertin	*Université Blaise Pascal, Clermont-Ferrand*
Bill Bertozzi	*Massachusetts Institute of Technology*
Louis Bimbot	*Institut de Physique Nucléaire, Orsay*
Tim Black	*Massachusetts Institute of Technology*
Werner Boeglin	*Florida International University*
Alexander Borissov	*University of Glasgow*
Ed Brash	*University of Regina*
Vincent Breton	*Université Blaise Pascal, Clermont-Ferrand*
Herbert Breuer	*University of Maryland*
Etienne Burtin	*DAPNIA/SPhN, CEA, Saclay*
John Calarco	*University of New Hampshire*
Alexandre Camsonne	*Université Blaise Pascal, Clermont-Ferrand*
Larry Cardman	*Jefferson Laboratory*
Gordon D. Cates	*University of Virginia*
Christian Cavata	*DAPNIA/SPhN, CEA, Saclay*
Zhengwei Chai	*Massachusetts Institute of Technology*
George Chang	*University of Maryland*
Ting Chang	*University of Illinois*
Nicholas Chant	*University of Maryland*
Jian-Ping Chen	*Jefferson Laboratory*
Seonho Choi	*Seoul National University, Korea*
Eugene Chudakov	*Jefferson Laboratory*
Steve Churchwell	*Duke University*
Evaristo Cisbani	*INFN/Sezione Sanità*
Leon Cole	*Hampton University*
Luminita Coman	*Florida International University*
Marius Coman	*Florida International University*
Brandon Craver	*Univ. of Virginia*
Benjamin Crowe	*North Carolina Central University*

Francesco Cusanno	*INFN/Sezione Sanità*
Dan Dale	*University of Kentucky*
Areg Danagoulian	*University of Illinois*
Nathalie Degrande	*Gent State University*
Raffaele De Leo	*INFN/Sezione Bari*
Alexandre Deur	*Jefferson Lab*
Nicole d'Hose	*DAPNIA/SPhN, CEA, Saclay*
Rachele di Salvo	*INFN/Sezione Roma2*
Pibero Djawotho	*College of William and Mary*
Frank Dohrmann	*Argonne National Laboratory*
Jean-Eric Ducret	*DAPNIA/SPhN, CEA, Saclay*
Dipangkar Dutta	*Duke University/TUNL*
Kim Egiyan	*Yerevan Physics Institute*
Martin B. Epstein	*California State University*
Stephanie Escoffier	*DAPNIA/SPhN, CEA, Saclay*
Catherine Ferdi	*University of Clermont Ferrand*
Robert Feuerbach	*Jefferson Lab*
Mike Finn	*College of William and Mary*
Kevin Fissum	*University of Lund*
Helene Fonvieille	*Université Blaise Pascal, Clermont-Ferrand*
Bernard Frois	*DAPNIA/SPhN, CEA, Saclay*
Salvatore Frullani	*INFN/Sezione Sanità*
Haiyan Gao	*Duke University*
Franco Garibaldi	*INFN/Sezione Sanità*
Ashot Gasparian	*Hampton University*
Gagik Gavalian	*Old Dominion University*
Olivier Gayou	*Massachusetts Institute of Technology*
Shalev Gilad	*Massachusetts Institute of Technology*
Ron Gilman	*Rutgers, The State University of New Jersey*
Alexander Glamazdin	*Kharkov Institute of Physics and Technology*
Charles Glashausser	*Rutgers, The State University of New Jersey*
Jackie Glister	*Saint Mary's University*
Javier Gomez	*Jefferson Laboratory*
Victor Gorbenko	*Kharkov Institute of Physics and Technology*
Tim Gorringe	*University of Kentucky*
Keith Griffioen	*College of William and Mary*
David Hamilton	*University of Glasgow*
Ole Hansen	*Jefferson Laboratory*
David Hayes	*Old Dominion University*
Bill Hersman	*University of New Hampshire*
Doug Higinbotham	*Jefferson Laboratory*
Wendy Hinton	*Old Dominion University*
Richard Holmes	*Syracuse University*
Harry Holmgren	*University of Maryland*

Tim Holmstrom	*College of William and Mary*
Maurik Holtrop	*University of New Hampshire*
Edik Hovhannisyan	*Yerevan Physics Institute*
Calvin Howell	*Duke University*
Garth Huber	*University of Regina*
Charles Hyde-Wright	*Old Dominion University*
Hassan Ibrahim	*Old Dominion University*
Ru Igarashi	*University of Saskatchewan*
Sebastian Incerti	*Temple University*
Mauro Iodice	*INFN/Sezione Sanità*
Riccardo Iommi	*INFN/Sezione Sanità*
Dave Ireland	*University of Glasgow*
Kees de Jager	*Jefferson Laboratory*
Stephanie Jaminion	*Université Blaise Pascal, Clermont-Ferrand*
Steffen Jensen	*California Institute of Technology*
Yi Jiang	*University of Science and Technology of China (USTC)*
Xiaodong Jiang	*Rutgers, The State University of New Jersey*
Cathleen Jones	*California Institute of Technology*
Mark K. Jones	*Jefferson Laboratory*
Seigo Kato	*Yamagata University*
Mina Katramatou	*Kent State University*
Lisa Kaufman	*University of Massachusetts*
James Kellie	*University of Glasgow*
James Kelly	*University of Maryland*
Sophie Kerhoas	*DAPNIA/SPhN, CEA, Saclay*
Armen Ketikyan	*Yerevan Physics Institute*
Kouichi Kino	*Tohoku University*
Norm Kolb	*University of Saskatchewan*
Ameya Kolarkar	*University of Kentucky*
Ioannis Kominis	*Princeton University*
Wolfgang Korsch	*University of Kentucky*
Serge Kox	*Institut des Sciences Nucléaires, Grenoble*
Alexander Kozlov	*University of Regina*
Kevin Kramer	*College of William and Mary*
Laird Kramer	*Florida International University*
Elena Kuchina	*Rutgers University*
Krishna S. Kumar	*University of Massachusetts*
Gerfried Kumbartzki	*Rutgers, The State University of New Jersey*
Geraud Lavessiere	*Université Blaise Pascal, Clermont-Ferrand*
John LeRose	*Jefferson Laboratory*
Mark Leuschner	*University of New Hampshire*
David Lhuillier	*DAPNIA/SPhN, CEA, Saclay*
Richard Lindgren	*University of Virginia*
Ken Livingston	*University of Glasgow*
Nilanga Liyanage	*University of Virginia*
George Lolos	*University of Regina*

Robert Lourie	*Renaissance Technology*
Hai-jiang Lu	*University of Science and Technology of China (USTC)*
Richard Madey	*Kent State University*
Kazushige Maeda	*Tohoku University*
Vahe Mamyan	*Yerevan Physics Institute*
Mark Manley	*Kent State University*
Demetrius Margaziotis	*California State University*
Pete Markowitz	*Florida International University*
Jacques Marroncle	*DAPNIA/SPhN, CEA, Saclay*
Jacques Martino	*SUBATECH, IN2P3, Nantes*
Samvel Mayilyan	*Yerevan Physics Institute*
Kathy McCormick	*Pacific Northwest National Lab*
David Meekins	*Jefferson Laboratory*
Zein-Eddine Meziani	*Temple University*
Bob Michaels	*Jefferson Laboratory*
Bernard Michel	*Univ. of Clermont-Ferrand*
Brian Milbrath	*Eastern Kentucky University*
Wilson Miller	*University of Virginia*
Joseph Mitchell	*Renaissance Technology*
Bryan Moffit	*College of William and Mary*
Peter Monaghan	*Massachusetts Institute of Technology*
Jean Mougey	*Institut des Sciences Nucléaires, Grenoble*
Pierre Moussiegt	*ISN Grenoble*
Carlos Munoz-Camacho	*DAPNIA/SPhN, CEA, Saclay*
Sirish Nanda	*Jefferson Laboratory*
Alan Nathan	*University of Illinois*
Vladimir Nelyubin	*St. Petersburg Nuclear Physics Institute*
Damien Neyret	*DAPNIA/SPhN, CEA, Saclay*
Dima Nikolenko	*Budker Institute of Nuclear Physics*
Blaine Norum	*University of Virginia*
Zisis Papandreou	*University of Regina*
Kent Paschke	*University of Massachusetts*
J.C. Peng	*University of Illinois*
Lubomir Penchev	*College of William and Mary*
Charles Perdrisat	*College of William and Mary*
Gerassimos G. Petratos	*Kent State University*
Artush Petrosyan	*Yerevan Physics Institute*
Eli Piasezky	*Tel Aviv University*
Stephane Platchkov	*DAPNIA/SPhN, CEA, Saclay*
Roman Pomatsalyuk	*Kharkov Institute of Physics and Technology*
Dan Protopopescu	*University of Glasgow*
Andrew Pucket	*Massachusetts Institute of Technology*
Vina Punjabi	*Norfolk State University*
Thierry Pussieux	*DAPNIA/SPhN, CEA, Saclay*

Issam Qattan	*North-Western University*
Xin Qian	*Duke University*
Gilles Quéméner	*Institut des Sciences Nucléaires, Grenoble*
Igor Rachek	*Budker Institute of Nuclear Physics*
Ronald Ransome	*Rutgers, The State University of New Jersey*
Brian Raue	*Florida International University*
Juerg Reinhold	*Florida International University*
Bodo Reitz	*Jefferson Laboratory*
Yves Roblin	*Jefferson Laboratory*
Rikki Roché	*Old Dominion University*
Mike Roedelbronn	*University of Illinois*
Oscar Rondon	*University of Virginia*
Guenther Rosner	*University of Glasgow*
David Rowntree	*Massachusetts Institute of Technology*
Gary Rutledge	*TRIUMF*
Marat Rvachev	*Massachusetts Institute of Technology*
Franck Sabatie	*DAPNIA/SPhN, CEA, Saclay*
Arun Saha	*Jefferson Laboratory*
Teijiro Saito	*Tohoku University*
Adam J. Sarty	*Saint Mary's University*
Ralph Segel	*Northwestern University*
Andrei Semenov	*Kent State University*
Albert Shahinyan	*Yerevan Physics Institute*
Ran Sheyor	*Tel Aviv University*
Simon Sirca	*Massachusetts Institute of Technology*
Karl Slifer	*University of Virginia*
Timothy Smith	*University of New Hampshire*
Patricia Solvignon	*Temple University*
Pavel Sorokin	*Kharkov State University*
Paul A. Souder	*Syracuse University*
Steffen Strauch	*GUniversity of South Carolina*
Ramesh Subedi	*Kent State University*
Riad Suleiman	*Massachusetts Institute of Technology*
Vincent Sulkovsky	*College of William and Mary*
Jeff Templon	*NIKHEF*
Tatsuo Terasawa	*Tohoku University*
Neil Thompson	*Univ. of Glasgow*
Luminita Todor	*Carnegie Mellon University*
H. Tsubota	*Tohoku University*
Hiroaki Ueno	*Yamagata University*
Paul E. Ulmer	*Old Dominion University*
Guido Urciuoli	*INFN/Sezione Sanità*
Antonin Vacheret	*DAPNIA/SPhN, CEA, Saclay*
Luc Van de Hoorebeke	*Gent State University*
Robert Van de Vyver	*Gent State University*

Pascal Vernin	*DAPNIA/SPhN, CEA, Saclay*
Branislav Vlahovic	*North Carolina Central University*
Hakob Voskanyan	*Yerevan Physics Institute*
Eric Voutier	*Institut des Sciences Nucléaires, Grenoble*
Richard Walter	*Duke University*
Kebin Wang	*University of Virginia*
John Watson	*Kent State University*
Dan Watts	*University of Glasgow*
Larry Weinstein	*Old Dominion University*
Richard Wilson	*Harvard University*
Krishni Wijesooriya	*Argonne National Laboratory*
Bogdan Wojtsekhowski	*Jefferson Laboratory*
Hong Xiang	*Harvard Medical School*
Wang Xu	*Massachusetts Institute of Technology*
Yunxiu Ye	*University of Science and Technology of China (USTC)*
Xiaohui Zhan	*Massachusetts Institute of Technology*
Jianguo Zhao	*General Electric*
Xiaochao Zheng	*Massachusetts Institute of Technology*
Shuhua Zhou	*China Institute of Atomic Energy (CIAE)*
Lingyan Zhu	*University of Illinois*
Xiaofeng Zhu	*Duke University*
Piotr Zolnierczuk	*University of Kentucky*

5 Publications

6 Theses